2017-01-01

Cycling Of Gypsiferous White Sands Aerosols In The Shallow Critical Zone At White Mountain, New Mexico

Patrick Richard Rea
University of Texas at El Paso, patrick.r.rea@gmail.com

CYCLING OF GYPSIFEROUS WHITE SANDS AEROSOLS IN THE SHALLOW CRITICAL ZONE AT WHITE MOUNTAIN, NEW MEXICO

PATRICK R. REA

Master's Program in Geology

APPROVED:

Lixin Jin, Ph.D., Chair

Thomas Gill, Ph.D.

Jorge Gardea-Torresdey, Ph.D.

Charles Ambler, Ph.D.
Dean of the Graduate School

Dedication:

To Russell Pellmann.

CYCLING OF GYPSIFEROUS WHITE SANDS AEROSOLS IN THE SHALLOW CRITICAL ZONE AT WHITE MOUNTAIN, NEW MEXICO

by

PATRICK REA, B.S.

THESIS

Presented to the Faculty of the Graduate School of

The University of Texas at El Paso

in Partial Fulfillment

of the Requirements

for the Degree of

MASTER OF SCIENCE

Department of Geological Sciences

THE UNIVERSITY OF TEXAS AT EL PASO

December 2017

ACKNOWLEDGEMENTS

I would firstly like to thank my advisor, Dr. Lixin Jin, for her patience and assistance in developing my experimental and writing abilities culminating in this text. I would also like to thank the other two members of my committee, Dr. Thomas Gill and Dr. Jorge Gardea-Torresdey for their mentorship and suggestions.

I am thankful for all the assistance I received in the lab, especially Dr. Lin Ma, as well as my colleagues Sandra Garcia, Anna Ortiz, Syprose Nyachoti, Mercedes Navarro-O'Hara, Jaime Enriquez, and Karen Valles. Thank you to everyone who provided assistance in the field, especially David Bustos and the staff at White Sands National Monment. I also appreciate the assistance in the field provided by students in the geology department and friends of the department, including Alex Eddy, Nick Tischio, and Joann Pinkley.

Thank you to Annette Veilleux, Kristen Gonzalez, Joel Gilbert, and everyone else in the office for their logistical support. Thank you to my other colleagues in the geology department for career, academic, or personal advice, especially those who helped with the 2016 Imperial Barrel Award team and my involvement at NASA.

Lastly, I would like to express my sincere thanks to my family for their support from across the country. Thank you to Maria for your love and patience – and to the rest of our family – Chai, Micah, and Cascade, for bringing joy and completeness to our home and lives.

ABSTRACT

Dry deposition significantly affects evolution of the critical zone by nutrient supply and contributing to soil genesis. Dust influx and cycling in soils are difficult to quantify because dust sources can be chemically similar to local soils. White Sands, New Mexico, emits gypsum dust with a unique chemical and isotopic signature, providing an opportunity to investigate dust deposition and its movement in soils. This study evaluated the mobility of White Sands dust particles in the critical zone at White Mountain, New Mexico, a highland 100km downwind. Four soil profiles were collected over limestone, igneous, mixed limestone and dolostone, and sandstone bedrocks, as well as leaves of local grass, shrubs, cacti, and pines. Dust, White Sands gypsum, and bedrock, considered as end members of soil calcium, were collected. All samples were analyzed chemically, mineralogically, and isotopically ($^{87}Sr/^{86}Sr$).

Depth variation in bulk soil chemistry at the study sites was mostly controlled by weathering over carbonate substrates, and by bulk dust addition over siliciclastic ones. White Sands, making up only a small portion of soil mass, dominantly controlled the Ca/Sr ratios, SO_4 concentrations, and $^{87}Sr/^{86}Sr$ ratios in water leachable fractions of the soils. Dust samples contained more soluble Ca and SO_4 than soils, suggesting high mobility of these soluble ions. For water-leachable fraction of the soils, Ca concentrations and the Sr/Ca ratio increased with depth as gypsum dissolved and reprecipitated as it reaches the impermeable bedrock-soil interface. The residence time of White Sands-derived gypsum in soil profiles was estimated to be approximately 66 years for Ca, and 83 years for SO_4.

The $^{87}Sr/^{86}Sr$ ratios in plants varied among plant types, primarily controlled by root depth, and dominantly sourced from dust. Although variation in Ca and Sr concentrations within the plants were largely controlled by plant type, concentrations of other elements were likely

controlled by other variables such as vegetation cover and geomorphology. Overall, tracking White Sands dust input to the soil has provided better understanding of gypsum's potential effects and the effects of long-distance dust transport on critical zone dynamics and sources of bioavailable plant nutrients.

TABLE OF CONTENTS

LIST OF TABLES

LIST OF FIGURES

1. INTRODUCTION

The critical zone is defined as the near surface environment where essential ecosystem interactions of rock, soil, water, and the atmosphere occur (Tchakerian and Pease 2015). The critical zone's composition, structure, evolution, and functions differ from arid to humid regions. Its characteristics are determined externally through chemical weathering and atmospheric deposition inputs and internally through cycling via precipitation and biology. Dry deposition is particularly important in arid ecosystems and controls the inputs which are ultimately cycled within critical zone environments (Capo and Chadwick 1999). Thus, changes of nutrient inputs through dust can have a profound effect on environmental dynamics (Reynolds *et al.,* 2006; Swap *et al.,* 1992).

Dust production and transportation are disproportionately sourced from drylands. They constitute 35% of the earth's land surface, and thus, significantly affect global nutrient cycling (Knippertz and Stuut 2014; Kumar *et al.,* 2014). As an example, the critical zone nutrient budget has been shown to be affected by dust from the Saharan Desert in reaching the Amazon (Abouchami *et al.,* 2013; Brantley *et al.,* 2007; Reynolds 2001, 2006). Other instances of aerosol input defining elemental additions include dust from the Mojave reaching the Colorado Plateau (Lawrence *et al.,* 2013), Saharan influence in the Andes mountains (Boy and Wilcke 2007), Asian and regional dust influence on nutrient cycles in the Sierra Nevada of California (Aciego et al., 2017), and Great Basin dusts reaching surrounding mountains (Gill 1996; Hoidale 1968; Marchand 1970). Primary productivity in many of these ecosystems is limited by distant arid aerosol flux and composition (Swap *et al.,* 1992).

However important, dust point source inputs to distant ecosystems are difficult to quantify because they generally come from multiple indistinguishable non-point sources mixing together

in short and long-distant transport (Derry and Chadwick 2007) . As dusts move further downwind, they become well mixed and mirror global or regional compositions (Bozlaker *et al.,* 2013; Trapp *et al*., 2010.) Deposition rates and dust composition can be spatially heterogeneous on small and regional scales (Hahnenberger and Nicoll, 2012; Huneeus *et al.*, 2011; Perez and Gill 2009; Rivas 2014). Long-distance aerosol transport and composition are more directly consequential in arid critical zones (Tchakerian and Pease 2015). In these dryland soils, long-range dusts can provide essential nutrients, especially in the form of soluble salts (Waterfall 1946). To model deposition and cycling of dusts in these regions, input end members with different chemical signatures than local soils must be isolated (Arendt *et al.*, 2015). Even if potentially isolated as a chemically distinctive end member, dust generally contains many other regional or point-source end members within its aggregate composition that are often relatively similar.

In the Tularosa basin of New Mexico, the White Sands produce a visible, intense, and frequent gypsiferous dust plume that is chemically unique from local aerosols (White et al., 2015; Baddock *et al.,* 2011, 2016; Figure 1). The prevailing winds from the southwest transport the dust to the east and northeast into the Sacramento and White Mountains (Fryberger 2001; White *et al.,* 2015). The White sands are comprised of a playa (Alkali Flat) and lake (Lake Lucero), representing the remnants of Pleistocene Lake Otero, with an associated gypsum dune field stretching downwind (Allmendinger 1973; Fryberger 2001). The gypsum dunes are derived from aeolian deflation and transport of evaporitic sands from the evaporated playa/lake system (Allmendinger 1973; Kocurek *et al.,* 2007; Langford *et al.,* 2016; Rivera *et al.,* 2010; Szynkiewicz *et al.,* 2010). Initiation of dune field formation dates to the beginning of the Holocene (Kocurek *et al.,* 2007; Langford 2016). The sands are a major source of dust in the

American Southwest and make the Tularosa basin and its surrounding ecosystems a natural laboratory for dust studies (Baddock *et al.,* 2011, 2016; Langford *et al.,* 2016; Prospero *et al.,* 2002; Rivera *et al.,* 2010; White *et al.,* 2015).

The White Mountain-White Sands region in New Mexico satisfies several conditions that allow specific dust sources to be isolated in soils: 1) Geochemical differences between depositing dust and chemically weathered soils, 2) Distinctive aerosol sources within bulk dry deposition, 3) Sufficiently intense and regular source of dust depositing a detectable signal into soils. Because of these circumstances, it is possible to isolate and trace three contributors to shallow soils at the study area: background dust, White Sands dust, and bedrock through chemical weathering (Figure 2).

In this study, I aim to characterize the behavior of specific end members within shallow soils at White Mountain. These end members include background dust, local bedrock, and White Sands dust component, with a special focus on the macronutrient calcium. Strontium isotopes, elemental chemistry, and mineralogy analyses are used on bulk soil and soil leachate fractions (isolating salt components) to characterize end members and determine a total calcium budget through soil profiles. This work will give a more complete picture of calcium fluxes and dynamics in gypsum-impacted active critical zone reservoirs, and will describe potential impacts and the mobility of atmospherically deposited salt. Three specific goals have been defined: 1) to evaluate atmospheric versus bedrock input on genesis of bulk soils using elemental, isotopic and mineralogical characteristics, as well as those of dust and gypsum end-members, 2) to investigate the mobility of gypsum dust within the soil profiles through investigation of soil leachates (water leachable fraction), and 3) to identify calcium sources in plants from different end members using elemental ratios (Ca/Sr) and isotopic ratios ($^{87}Sr/^{86}Sr$).

2. STUDY SITES

White Sands emit a regular and significant plume northeasterly towards White Mountain (White *et al.,* 2015.) The gypsum dune field is a result of the exposure, weathering, and accumulation of gypsum from the Permian Yeso formation in the Tularosa basin (Fryberger 2001.) The variation of White Sands dune structure, dust emission, and chemistry is controlled by a variety of kinetic and hydrological variables (White *et al.*, 2015.)

Uplift and subsidence fault blocks results in a large relief between White Mountain, the Tularosa basin to the west, and the study site in the basin directly east in the Ruidoso fault zone. Specifically, White Mountain lies 2340m higher than the Tularosa basin to the west as a result of early to middle Tertiary volcanism and subsequent Rio Grande rift faulting (Kelley and Thompson 1964). Numerous largely monzonitic laccoliths and stocks are scattered about the area and caused extension and faulting in the late Paleozoic and Mesozoic limestones and sandstones. The study area bounded within the basin has 5°C (~30%) lower average temperature and 0.64m (over twice as much) annual precipitation than the Tularosa basin on the other side of White Mountain (Climate Data 2016, Station RUIDOSO 1.7 WNW, NM US).

The vegetation types of the study area include madrean encinal pinyon-juniper woodland and semi-desert grasslands (Hanks and Dick-Pettle, 1974; Martin 1964; Vander Lee *et al.*, 2004). Because of increased precipitation relative to the region, the study area has a relatively active critical zone biologically and hydrologically. Additionally, dust input in the Chihuahuan Desert to the south at Las Cruces, New Mexico was estimated at 7 to 28 $g/m^2/yr$ (Perez 2008); in El Paso, Texas, further to the south, almost 200 $g/m^2/yr$ dust fall annually (Rivas et al., 2014). These sites only rarely receive dust from the White Sands, compared to the prevalence of White Sands Aeolian deposition at White Mountain (White et al., 2015). A large portion of dust

deposition in the Chihuahuan Desert occurs during isolated dust events (Perez and Gill, 2009; Rivera Rivera et al., 2010; White *et al.,* 2015). The spatial and temporal heterogeneity of dust deposition over short distances makes deposition rates at White Mountain difficult to estimate. Significant aerosol input from White Sands and surrounding arid lands gives an opportunity to study dust interactions in active critical zone environments with biota and precipitation.

3. METHODS

3.1. Site Selection and Sample Collection

Soil sampling sites in the White Mountain area were selected based on slope, aspect, bedrock substrate, and proximity to human interference as discussed below. Sites facing southwest (primary direction of dust transport) or lying on the top of ridges were chosen because these soils would be expected to receive more significant dust deposition from White Sands than those from east-facing slopes (White *et al.*, 2015). Two sites (A, D) were placed atop ridges; two others (B, C) were on steep vegetated slopes and shallow grassy slopes, respectively, facing the southwest towards White Sands (Figure 1). Sites were selected over bedrock substrates that vary in both composition and reactivity (Table 1). Lithologies were identified using the New Mexico Bureau of Geology and Mineral Resources' state geologic map and field observation: Site A lies over Artesia limestone; B, Tertiary igneous rocks; C, San Andres mixed limestone and dolostone; and D, Mesa Verde sandstone (New Mexico Bureau of Geology and Mineral Resources 2003). Sites A, B, and C surround Sierra Blanca Regional Airport to the northwest, west, and southeast, respectively; site D is 20km to the northwest, near Capitan, NM (Figure 1). These sites are away from anthropogenic interference, including major roads and other contamination sources.

At each site a soil pit was dug and soil samples were collected at 5cm intervals. Soil pits ideally reach bedrock, and if not, be at least 20 cm deep. Rock fragments were collected at the bottom of the soil pits as bedrock. Leaves from most prevalent cacti, grasses, shrubs, and pines were gathered, identified, and analyzed for each site.

To collect dust samples, two vertical falling-dust traps were installed 1.5m above ground at sites A and C using USGS protocol (Reheis and Kihl 1995). Traps were constructed with marbles secured with chicken wire in a Teflon-coated cake pan (Figure 3). The pan is secured to

a U-post driven into the ground. Each sample collection required traps to be taken off, dismantled, and replaced on site. Between each collection, marbles are removed from pans and stored for dust collection using deionized water (DI) rinsing and subsequent evaporation in storage containers. Data from the nearby White Mountain sampler (WHIT1) in the IMPROVE national aerosol monitoring network (White *et al.,* 2015), which collects and measures the fine component of aerosols (<2.5 μm), was downloaded. Precipitation data from the National Atmospheric Deposition Program's National Trends Network (NADP NTN) dataset were downloaded for Mayhill site in Otero County, ~60km to the southwest of the study sites.

To collect and characterize dust end-member derived from the White Sands, surface sediment samples were collected within the White sands in areas considered most likely to mobilize and become sources of dusts for long-range transport. Distinct geomorphologies and locations in the White Sands were chosen to constrain potential end members of White Sands chemistry, recognizing that the episodic dust events and spatiotemporal yields a range of chemical White Sands signatures (White *et al.,* 2015). Special focus was paid to erosional interdunes and dune slip faces with small wind ripples, which are shown to be both fine-grained and scarcely vegetated (Langford *et al.,* 2016). Nine samples were gathered from barchan and parabolic dunes and interdunes, loose sediments below gypsum crusts, as well as flat areas without dunes (Figure 1; Table 1).

3.2. Sample Preparation and Analyses

3.2.1. Soil, dust and rock preparation

Rock fragments and <2mm soils were separated from bulk soil, homogenized and ground down to #100 mesh (< 150μm). Dust samples contained a significant amount of organic matter and clung to the surfaces of dust collectors. DI water was used to clean the pan and remove the

dust; the mixture was gathered in a beaker, and then evaporated overnight. The evaporated solid was collected, weighed, and loss on ignition (LOI) was performed at 550°C to estimate organic matter contents.

3.2.2. Soil, dust, and rock analysis: major element chemistry

To prepare for elemental analysis, 100±0.5mg of ground dust, soil, or rock samples were weighed, mixed with 1000±2mg lithium metaborate, and digested in a furnace at 950°C for 10 minutes using methods developed by Surr *et. al* (1966), Medlin *et al.* (1969), Ingamells (1970), and Feldman (1983) (Appendix A). After completely molten, the samples were re-dissolved in 5% HNO_3 and diluted 1:10 with 5% HNO_3. This solution was measured on a Perkin Elmer 5300DV inductively coupled plasma optical emission spectrometer (ICP-OES) for major elements and several trace elements. 20 rock standards were digested and used for calibration. Duplicates were run to measure experimental precision, and two procedure blanks were run for quality control and assurance.

Almost all major elements analyzed for this study had less than 5% variance between procedure and analytical duplicates. Up to 6% difference between duplicates is observed for CaO. However, trace metals had higher uncertainties: up to 11% difference (average 3%) is observed in Sr, and 33% in Ba (Appendix C). Procedure blank was low, with sum of all elements being less than 1 wt% after the identical lithium metaborate procedure was performed.

3.2.3. Soil and rock analysis: mineralogy via X-Ray Diffraction

Ground rocks and soils were qualitatively analyzed for mineralogy using X-ray powder diffraction (XRD) to help identify mineral phases and evaluate relative depletion or enrichment of these phases as rock weathering progresses and dust is added. Finely ground samples were prepared on a smear thin section and analyzed on a Rigaku XRD. Samples were run from 10° to

65° (2-theta) at a 0.03° step size and 1.5°/min scan speed. EVA DIFFRAC Suite software was used to identify peaks using the ICDD PDF-2 2008 release XRD database.

3.2.4. Soil analysis: Carbon and sulfur content

Bulk soil samples were analyzed for total carbon, organic carbon, and total sulfur. Approximately 0.25g of soil was combusted at 1350 °C with 1g of combustion aid (com-aid) on a LECO SC632 Sulfur/Carbon determinator. Two standards with different C/S concentrations (LECO 502-062 and LECO 502-814) were used for calibration and quality assurance. Organic carbon was quantified after carbonates were removed with 1:1 HCl solution and samples were dried in the oven at 60 °C.

3.2.5. Soil analysis: Sr isotopes

100mg of soil or rock samples were put into the clean Teflon beakers and digested using concentrated hydrofluoric and nitric acids. Solutions were evaporated and then redigested with boric and hydrochloric acid, before being evaporated again and re-dissolved in 3.5N nitric acid (Pett Ridge *et al.*, 2009). See appendix B for procedural details.

3.2.6. Water Leaching of soil and dust: Elemental Chemistry and Sr isotopes

The water soluble fraction isolated any evaporite salts, including gypsum from dust. A solid sample (soils, or dust) and water were weighed, mixed into a slurry via hand shaking for a minute, and then centrifuged at 3500 rpm for 10 minutes. The supernatant solution was filtered through a 0.45µm cellulose acetate syringe filter, and then analyzed for electric conductivity (EC) and pH using hand meters, for concentrations of major cations on an ICP-OES, for concentrations of anions on an ion chromatograph (IC, Dionex ICS-2100), and on a multi-collector ICP-mass spectrometer (MC-ICP-MS) for strontium isotopes.

For cation concentrations, leachate samples were diluted with DI water and then acidified using 3 drops of concentrated nitric acid before ICP-OES analysis. USGS reference standards M178, M182, and M210 were run as checks for quality control. Duplicate solution samples and procedure blank were run for quality assurance. Leachates were diluted with DI water before IC analysis for anion concentrations. The flow rate was set to 1 mL/min, the suppressor at 75 mA, and internal machine temperature at 30° C. A check standard was made from diluting alltech anion mix A and run along with unknown samples, a procedure blank and duplicates.

3.2.7. Plant analyses: major element chemistry and Sr isotopes

Plant leaves were rinsed with DI water, oven dried, and ground using a coffee grinder. 0.2g of a ground leaf sample was mixed with 5mL concentrated nitric acid, microwave digested using hot block acid digestion, then diluted to 50mL with DI water to a 5% nitric acid solution. The diluted solution was measured on the ICP-OES for concentrations of major and trace elements.

To prepare for strontium isotopes, vegetation samples were put into Teflon Parr bomb digestion containers with 6mL of concentrated nitric acid. Pressure built up for 24 hours at 100°C, and after cooling, samples were collected and evaporated. Dried samples were re-dissolved in 3.5N HNO_3 and centrifuged, and 1mL of sample was used for column chemistry.

3.2.8. Sr isotopes by MC-ICP-MS

Strontium isotope ratios ($^{87}Sr/^{86}Sr$) of leachates, dust, soil, rock, and plant samples were run on the Nu plasma HR Multi-collector ICP-MS (MC-ICP-MS) at the Department of Geological Sciences of the University of Texas at El Paso after digestion and elution of extraneous elements through a column chemistry procedure (Konter and Storm, 2014). Containers for the procedure require cleaning, with consecutive 1 day soaks of aqua regia (3:1 HNO_3: HCl solution,) Extran, 20% HCl, de-ionized water, and millipore (18MΩ) water. The prepared samples were run

through two leaching phases (one for plants) to extract strontium from samples that will be run on the MC-ICP-MS. The dissolved samples were put into a column filled with Eichrom Sr-resin; other elements were eluted out in a series of 3.5N nitric acid aliquots until the Sr is collected using 0.05N nitric acid. This procedure was done twice for each sample (only once for plants) to completely elute other elements, and between runs a sample was evaporated and re-dissolved in 3.5N nitric acid. A procedure blank was run to identify potential background voltage or systematic contamination when run on the MC-ICP-MS.

Standard SRM-987 was used to correct for machine drift and run after each set of 3 samples. Check standard BCR-2 was run with samples repetitively as well, with an average of 0.70500±0.00002 (n=4), within the certified value of 0.70502±0.0001.

4. RESULTS

4.1. Bulk soil/dust/rock chemistry, isotopes, and mineralogy

4.1.1. Major Element Chemistry

All elemental and isotopic data for bulk soil and rock samples were reported in Table 2. Calcium oxide increased dramatically with depth at site A (limestone; from 5.7 to 31.4 wt%) and at site C (limestone/dolostone; from 6.2 to 9.5 wt%), but remained low and relatively unchanged with depth at site B (diorite; from 2.0 to 2.1 wt%) and at site D (sandstone; from 0.8 to 1.3 wt%.) Other oxides (Fe_2O_3, Al_2O_3, K_2O, and Na_2O), dominant in silicate minerals, decreased in their abundance with depth at sites A and C. For instance, Al_2O_3 content decreased from 14.2 to 9.17 wt%, and from 15.0 to 12.7 wt% at site A and site C, respectively. In contrast, the Al_2O_3 content increased with depth at site B (16.4 to 18.3 wt%) and at site D (9.3 to 12.5 wt%). The MgO content decreased with depth at site A (1.2 to 0.9 wt%), remained relatively constant at site B and site C (1.2 to 1.3 wt%), and increased slightly with depth at site D (0.6 to 0.9 wt%).

Depth trends of Sr concentrations followed those of CaO in all four profiles (Table 2). Ca/Sr ratios increased with increasing depth in all four soil profiles (Table 2): 0.33 to 1.32 mol/mmol at site A, 0.09 to 0.11 mol/mmol at site B, 0.34 to 0.42 mol/mmol at site C, and 0.06 to 0.09 mol/mmol at site D. All Ca/Sr ratios of the deepest soil samples at bedrock-soil interface were similar as those observed in the corresponding bedrock.

The S contents for all samples were below detection limits (0.1 wt%). Check standards for carbon analyses were measured within < 1% relative error of the certified values. Organic carbon and inorganic carbon, assumed to be carbonates, were measured separately. Contents of organic carbon in soils decreased with depth in all four weathering profiles (Table 2). Inorganic carbon (difference between total carbon and organic carbon) increased with depth over sites with

carbonate bedrock. Inorganic carbon was stoichiometrically converted to calcite (sites A, B, D) or dolomite (site C) wt% based on minerals identified via XRD (Figure 4). site A (limestone) had a sharp increase of calcite mass below 25cm (up to 48 wt% calcite in soils); and site C (dolostone) had up to 11 wt% dolomite in soils. Inorganic carbon contents were much lower and mostly not detectable in soils and bedrock samples at site B and site D. Up to 61% of total calcium oxides measured at site A and up to 20% at site C were in carbonates at depth (Table 2).

4.1.2. Mineralogy

XRD spectra and major minerals identified were shown for bedrock and representative soils from four study sites, dust, and gypsum dune samples (Figures 4A, B, C, D and E). Site A showed nearly pure calcite in bedrock (Figure 4A). Towards soil surface, quartz and microcline peaks became more pronounced relative to calcite. The bedrock of site B contained predominantly quartz, plagioclase, and microcline (Figure 4B). The bedrock in site C was comprised of dolomite, calcite, quartz, and microcline (Figure 4C). Quartz and calcite increased in relative abundance towards soil surface. The bedrock in site D were dominated by quartz with minor microcline (Figure 4D). White Sands dune samples were comprised almost completely of gypsum; Lake Lucero sediments showed traces of halite and mirabilite (sodium sulfate) in addition to gypsum (Figure 4E). Bulk dust contained quartz, calcite, and K-feldspar (Figure 4E).

4.1.3. Bulk Soil Strontium isotopes

Bulk soil $^{87}Sr/^{86}Sr$ ratios varied between 0.7070 to 0.7089 at sites A, B, and C, but were much higher at site D (0.7103 to 0.7112) (Figure 5A; Table 2). The strontium isotope ratios were variable for the top 15 cm soils at site A, and decreased steadily from 0.7087 to 0.7079 in soils from 15cm to 50cm depth, with the $^{87}Sr/^{86}Sr$ ratio of limestone bedrock measured at 0.7083. The $^{87}Sr/^{86}Sr$ ratios in bulk soils at Site B generally decreased with depth from 0.7075 to 0.7070 with

more variability at top 15 cm, and the igneous bedrock had the $^{87}Sr/^{86}Sr$ ratio of 0.7072. At site C, the Sr isotope ratios in bulk soils varied little between 0.7074 and 0.7076, different from the bedrock at 0.7100. The $^{87}Sr/^{86}Sr$ ratios at site D increased in bulk soils with depth from 0.7103 to 0.7112, with a bedrock ratio of 0.7108.

4.2. Elemental and isotope data for soil leachates: water soluble fraction

4.2.1. pH and Electrical Conductivity (EC)

Data for water leachable fractions of soils including concentrations of major elements, pH and EC were reported in Table 3. Soil pH at site A varied between 6.7 and 7.2 over the limestone substrate, with a mean of 7.0. Site B, over tertiary diorite, had lower soil pH, ranging from 6.0 to 7.0, with a mean of 6.3. Site C, over mixed limestone and dolostone, had a similar soil pH range as site A, between 7.0 and 7.5 with a mean of 7.2. Soil pH at site D over sandstone, was slightly more acidic, and ranged from 6.0 to 6.5, with a mean of 6.4.

Soil: water ratios were slightly variable among sites A, B and C, ranging from 39 to 66 (g of soil per L of water), but much higher at site D (130 to 145 g soil per liter of water). So measured EC values in the water leachates cannot be directly compared. Even so, several observations can be made. The EC of the soil leachates were low, from 27 to 181 □s/cm. Except for the shallowest sample, soils at site D had the lowest EC values among four sites. The EC increased with depth at site A and site B, but for site D, higher EC was observed at soil surface.

The EC of dust leachate was much higher than soil EC, at 47.2 mS/cm. Similarly, even with very low solid to water ratio for dust samples, the leachates had much higher EC values than soils.

4.2.2. Major Element Chemistry in the soil leachates

For cations, the concentrations of dissolved calcium and strontium in check standards were within the certified values by an average of 3.4% and ±3.5%, respectively. Check standards were measured with 10% with reference values for all anions (1.5% for F^-, 8.8% for Cl^-, 4.4% for SO_4^{2-}, 2.4% for NO_3^-, and 5.7% for PO_4^{3-}).

The concentrations of anions and cations in leachates were converted to mg/kg soil. The water-soluble fractions showed trends similar to those of leachate EC, ranging from 17-34.2 mg/kg soil at site A, 21.8-28.7 mg/kg soil at site B, 33-43.8 mg/kg soil at site C, and 138-278 mg/kg soil at site D (Table 3). At sites A, B, and C, the dominant cations in soil leachates were Ca^{2+} and K^+; soils at site D in the water soluble fraction were dominated by Ca^{2+}, K^+, and Na^+ as cations. The Ca/Sr ratios (mol/mmol) in water soluble fraction of soils decreased with depth at all sites, from 1.4 to 0.2. A relatively higher Ca/Sr ratio was observed from 0-10cm soil in all sites, with a mean 0.6±0.4 mol/mmol. The Ca/Sr ratio of the water leachate was 0.4 mol/mmol in dust, 0.6 mol/mmol in White Sands dune samples, and 2.5 mol/mmol in the Lake Lucero sediment.

Concentrations of anions in water soluble fraction of soils ranged from 33.8-136.5 mg/kg soil at site A, 26.3-102.1 mg/kg soil at site B; 43.0-85.1 mg/kg soil at site C, and 22.9-69.5 mg/kg at site D (Table 3; Figure 7). The mean and standard deviation of the top 20cm soil were 47.0±17.5 mg/kg soil for site A, 55.4±28.7 mg/kg soil for site B, 51.8±6.1 mg/kg soil for site C, and 41.2±17.5 mg/kg soil for site D. Dust leachate total volume in bulk dust was substantially higher at 37 g/kg dust. The White Sands samples contained nearly all water soluble contents, ranging from 45-51 wt% anions, predominantly SO_4 (Table 3.)

Sulfate and chlorite were dominant anions in the soil leachates, followed by fluoride. Nitrate and phosphate were only important at soil surface. Total soluble anions increased in concentrations with depth, largely due to increasing SO_4 concentrations (Figure 7). The SO_4:Cl ratios (in equivalent basis) increased with depth from 0.44 to 3.71 at site A, 0.49 to 2.74 at site B, 1.03 to 2.61 at site C, and 0.13 to 2.31 at site D. The SO_4: Cl ratios were 0.6 in dust and ranged from 107 (Lake Lucero) to 790 (dune) in White Sands samples.

4.2.3. Water Leachate Strontium Isotopes

The Sr isotope ratios in water leachates of the White Sands samples had a narrow range between 0.7078 and 0.7079, except for Lake Lucero sediments (0.7087) (Table 3; Figure 5B). For the dust, the water leachate had a $^{87}Sr/^{86}Sr$ ratio of 0.7080. The $^{87}Sr/^{86}Sr$ in water leachates of soil samples varied little among sites and also with depth between 0.7078 and 0.7083 (0.7079±0.0001; n= 30).

4.3. Elemental and isotope data for plant samples

4.3.1. Major Element Chemistry

The same checks were used for soil leachates and plant digest samples. As reported above, concentrations of calcium and strontium were different from the certified values by an average of 3.4% and 3.5%, respectively (Table 3). Plant chemistry including Sr isotopes were reported in table 4. Total elements that were measured in plants (Al, Ca, Fe, K, Mg, Mn, Na, and Sr) ranged from 1.6±0.4 wt% at site A, 2.8±1.4 wt% at site B, and 4.8±2.5 wt% at site C (not measured at site D). Dominant elements in all plants from all sites were Ca (mean: 1.1 wt%), K (mean: 0.6 wt%), and Mg (mean: 0.2 wt%). Na (mean: 2.4 wt%) was only observed in plants of site C.

Calcium concentrations varied more between specific plant types than between sites. For example, Ca concentrations ranged from 0.26-0.52 wt% in grasses, but were much higher compared to 0.7-1.5 wt% in pines and shrubs. The highest Ca concentration of 3.2 wt% was observed in cactus sample from site B. Ca/Sr ratios (mol/mmol) ranged from 0.21-0.29 in grasses, 0.10-0.30 in pines, 0.25-0.55 in shrubs, and 0.27 in the cactus at site B. Within sites, shrubs have the highest Ca/Sr, grasses are intermediate, and pines are the lowest. One exception was BP1 (pine from site B) with a relatively higher Ca/Sr ratio of 0.3mol/mmol, different from other pines.

4.3.2. Plant Strontium Isotopes

The Sr isotope ratios were different between plant type and also among sites (Table 4; Figure 5b). Grasses typically had the highest $^{87}Sr/^{86}Sr$ ratios among all vegetation samples at each site: 0.7082, 0.7079, 0.7080, and 0.7090 for sites A, B, C, and D, respectively. Shrubs and pines had slightly lower ratios (shrubs: 0.7078, 0.7077, 0.7080, and 0.7081 at sites A, B, C and D; pines: 0.7077, 0.7077, 0.7079, and 0.7081 at sites A, B, C, and D). In all cases, isotopic values of plants at site D were the highest when compared to the same plant types at all other sites. The isotopic ratios at site C showed the least variation, and they never exceeded 0.7079 at site B.

5. DISCUSSION

The primary goal of this study is to track a specific dry deposition source (gypsum from White Sands) into and through soils and vegetation at a downwind highland deposition site (White Mountain) using geochemical and isotopic tools. Three specific goals have been defined: 1) to evaluate atmospheric versus bedrock input on genesis of bulk soils using elemental, isotopical and mineralogical characteristics, as well as those of dust and gypsum end-members, 2) to investigate the mobility of gypsum dust within the soil profiles through investigation of soil leachates (water leachable fraction), and 3) to identify calcium sources in plants from different end members using elemental ratios (Ca/Sr) and isotopic ratios ($^{87}Sr/^{86}Sr$).

5.1. Relative importance of atmospheric inputs and chemical weathering of bedrock in controlling soil genesis

5.1.1. Characterization of end members

Bulk critical zone soils are an aggregate of three end members: (1) soils formed by chemical weathering of bedrock or parent materials, (2) atmospheric inputs, which vary spatiotemporally, and (3) biota input, which is largely organic and not quantitatively analyzed in this study. Gypsum from White Sands is an important source of dust for White Mountains due to its regular and significant downwind transport (Figure 1). To constrain White Sands chemistry, samples were collected from a barchan and parabolic dunes and interdunes, a hill crest, and from gypsum flats on an east-west transect in the northernmost part of the dune field (Table 1; Figure 1). Sediments from Lake Lucero were also collected to better quantify White Sands chemical variation. In addition, dust was collected, aggregated and analyzed as a single end member gathered over two years (Appendix C).

Bedrock over the four sites was identified using geological map data, hand identification, qualitative mineralogy, and elemental data. Site A was over a nearly pure limestone substrate (93% calcite) with an $^{87}Sr/^{86}Sr$ ratio of 0.7083 and Ca/Sr of 2.67 mol/mmol (Table 2; Figure 4A; Figure 5A). Site B was over a diorite substrate containing alkali and plagioclase feldspars, with a $^{87}Sr/^{86}Sr$ ratio of 0.7072, and Ca/Sr ratio of 0.13 mol/mmol (Table 2; Figure 4B; Figure 5A). Bedrock at site C was identified as mixed limestone and dolostone, with a $^{87}Sr/^{86}Sr$ ratio of 0.7100 and Ca/Sr ratio of 0.51 mol/mmol (Table 2; Figure 4C; Figure 5A). Site D was over nearly pure sandstone with a $^{87}Sr/^{86}Sr$ ratio of 0.7108 and Ca/Sr of 0.03 mol/mmol (Table 2; Figure 4D; Figure 5A).

Bulk dust contained quartz, calcite, and K-feldspar, with an $^{87}Sr/^{86}Sr$ ratio of 0.7087 (Table 2; Figure 4E). White Sands dune samples were pure gypsum with a narrow range of $^{87}Sr/^{86}Sr$ ratios ranging from 0.7078-0.7079, and Lake Lucero sediments contained traces of mirabilite ($Na_2SO_4 \cdot 10H_2O$) and halite (NaCl) with a $^{87}Sr/^{86}Sr$ ratio of 0.7087 and Ca/Sr of 2.4 mol/mmol (Figure 4E; KellerLynn 2012).

5.1.2. Bulk Soil Chemistry Variation: Mass Transfer coefficient τ

Mobile elements (e.g., calcium, strontium or iron) or oxides were conventionally normalized to an immobile element such as titanium or zirconium in order to characterize mobility dynamics of these elements in soil profiles (Brantley *et al.*, 2007). The equation to calculate the mass transfer coefficient for a given element j is as follows:

$$\tau_{i,,j} = \left(\frac{C_{j,w}\ C_{i,p}}{C_{j,p}\ C_{i,w}}\right) - 1$$

where C is the concentration of an immobile (*i*) or a mobile (*j*) element in weathered (*w*) or parent (*p*) material. Characterization of τ depth profiles show typical trends that indicate unique geochemical behaviors for given mobile element *j*: 1) immobile if τ=0, 2) depleted by leaching if

τ <0, 3) added if τ >0, 4) mobilized at surface (τ <0) enriched at depth if (τ >0), or 5) biogenic profiles if (τ <0 at depth but τ >0 at surface) (Brantley *et al.,* 2007). Error in mass transfer coefficients was propagated using the following formula (Jin *et al.,* 2010):

$$\text{Error } (\tau) = (\tau+1)\sqrt{\left(\frac{d\mathrm{A}}{A}\right)^2 + \left(\frac{d\mathrm{B}}{B}\right)^2 + \left(\frac{d\mathrm{C}}{C}\right)^2 + \left(\frac{d\mathrm{D}}{D}\right)^2}$$

Where $\frac{d\mathrm{A}}{\mathrm{A}}, \frac{d\mathrm{B}}{\mathrm{B}}, \frac{d\mathrm{C}}{\mathrm{C}}, \frac{d\mathrm{D}}{\mathrm{D}}$ are the relative uncertainties in $C_{j,w}$, $C_{i,p}$, $C_{j,p}$, *and* $C_{i,w}$, respectively. For our soil samples, relative errors were assumed to be 5% in analyzing concentrations of major elements, and 10% in trace elements. It is also assumed that heterogeneity of the bedrock contributed little to C_i.

Using titanium as the immobile element (*i*), mass transfer coefficients were calculated for *j* (CaO, Sr, Na_2O, and MgO) and plotted as a function of depth for four soil profiles (Figure 7). CaO showed a depletion profile at site A, was slightly depleted in sites B and C relative to bedrock, but was greatly enriched at site D ($3 < \tau$). Similarly, Sr was depleted at site A, almost immobile at sites B and C, and enriched ($0.25 < \tau < 1.8$) in site D. MgO was depleted at sites A and D, and slightly enriched at sites B and C. Na_2O is immobile at site A, depleted at sites B and C (apart from 35-40cm,) and added at site D.

5.1.3. Profile characterization using chemical, isotopical, and mineralogical trends

At site A, bedrock weathering, i.e., calcite dissolution, was the primary control on bulk soil as observed through negative τ values, a decrease in inorganic carbon concentrations toward surface, and decrease of intensity of calcite peaks in XRD spectra at shallow soils (Table 2; Figure 4A; Figure 8). In addition, Ca/Sr and $^{87}Sr/^{86}Sr$ ratios of bulk soils changed with depth and converged on the bedrock values. The Ca/Sr ratio in bulk soils increased with depth from 0.3 mol/mmol at the surface to 1.3 mol/mmol around 50 and 60 cm below ground surface, moving

closer to the bedrock Ca/Sr ratio (2.7 mol/mmol). The $^{87}Sr/^{86}Sr$ values down profile varied from 0.7087 around 15 to 20 cm to 0.7084 around 40 to 45cm, converging on the bulk bedrock value of 0.7083. Toward ground surface at Site A, soils were more chemically and mineralogically altered through weathering of calcite. Indeed, quartz and K-feldspar had larger peaks in XRD towards the surface along with an increase in absolute concentrations of their associated elements increased (K, Al, and Si). This increase in siliciclastic minerals was accompanied by decreases in concentrations of the carbonate-associated elements (Ca and C) (Table 2; Figure 4A). Thus the Ca/Sr and $^{87}Sr/^{86}Sr$ ratios observed at surface were indicative of silicate mineral end-member – and at depth - Ca/Sr and $^{87}Sr/^{86}Sr$ ratio modification indicated a mixing of carbonate and silicate mineral end-members.

Site C was also overlaying carbonate rocks (mixed dolostone and limestone), but with addition of about 80% silicate minerals. Compared to bedrock, soils were almost completely depleted of dolomite, but more enriched in calcite (Figure 4C). However, mass transfer coefficients of carbonate-bearing elements (CaO, MgO and Sr) were all immobile. Thus, it is possible that bedrock-sourced dolomite dissolved to form calcite. This transition seemed to be abrupt right around the bedrock-soil interface as observed by dramatic shifts in Ca/Sr ratio and $^{87}Sr/^{86}Sr$ (Figure 5C; Figure 8). Above this interface, Ca/Sr and $^{87}Sr/^{86}Sr$ ratios were almost constant in the soils (Figure 5).

The soil profiles at site B were developed on diorite with relatively low CaO concentrations (Table 2). The primary Ca-bearing mineral in the diorite was plagioclase (Figure 4B). The mass transfer coefficients of calcium were close to 0, indicating the immobile nature of Ca and thus slow weathering of plagioclase (Table 2; Figure 7A). The Ca/Sr ratios of the bulk soils varied little with depth (0.09-0.13 mol/mmol), and increased slightly at the top soil sample (Figure 5B).

The $^{87}Sr/^{86}Sr$ ratios increased gradually toward surface, with sharp peak at 10 cm soil depth (Figure 5A). Both Ca/Sr and $^{87}Sr/^{86}Sr$ ratios at shallower soils shifted towards dust and White Sands end-members, probably indicative of their inputs.

The soils at site D were developed on sandstone with low CaO contents and minimal chemical weathering; thus variation in soil chemistry was controlled by dust inputs (Figure 4D, Figure 8). Positive τ values indicated that CaO, Sr, MgO and Na_2O were enriched in soils (Figure 8). The Ca/Sr remained relatively constant around 0.08 mol/mmol (Table 2; Figure 5C), but the $^{87}Sr/^{86}Sr$ ratios decreased gradually towards the atmospheric end members at soil surface, indicating that atmospheric deposition dominates chemistry at this site.

In summary, soils at site A and site D represented two extreme conditions in this study. Calcite was quite reactive at site A, depleting Ca and making Ca inputs from dust invisible through bulk soil analysis (Figure 4; Figure 8). In contrast, sandstone at site D had low CaO contents and was not reactive, making it possible to observe Ca enrichment at surface, presumably derived from dust. Sites B and C are mixed systems with soil Ca and Sr being added by dust but depleted by chemical weathering. CaO and Sr behaved similarly in all profiles, suggesting similar sources and mobility between these two elements. The absence of significant dust signals in bulk soil at sites A and C indicated that bulk CaO and Sr in these sites are greatly modified by bedrock weathering. Dust signals appeared in site B and were especially strong in site D, suggesting that bulk dust was a significant contributor to soil chemistry, but the variance between the two sites indicated that atmospheric inputs were not the only soil chemistry contributor.

Due to the small sample size, no elemental data were collected for bulk dust, except for Sr isotopes. Thus, it was impossible to pinpoint the Ca/Sr ratios in dust. However, top soils at sites

B and D, where dust contribution was visible, shed lights on potential chemical signatures of bulk dust. For example, Ca/Sr in soils at site B ranged from 0.09 mol/mmol to 0.14 mol/mmol from soil to bedrock (Figure 5c). This would suggest that the Ca/Sr ratio for dust should be lower than 0.14 mol/mmol. Similarly, Ca/Sr ratios in soils at site D ranged from 0.09 to 0.06 mol/mmol with a bedrock signature of 0.03 mol/mmol, also corroborating that the Ca/Sr ratio of dust should be low (<0.1 mol/mmol). When constraining dust Ca/Sr ratios, it is important to consider that the Ca/Sr ratio of dust, once deposited on soils, could fractionate via biological processes or precipitation of secondary calcite (Neher *et al.*, 2009). Carbonate, present in the dust as observed through XRD (Figure 4), was not detected in the soil profiles at site B or D, suggesting calcite was quickly dissolved.

Although the elemental and isotopic data clearly indicated the presence of dust, especially at site B and site D, the bulk soil analyses could not differentiate background dust versus gypsum dust from White Sands. It was necessary to utilize a water leaching procedure to isolate the soluble portion of this dust and investigate the mobility of this dust component in the soils.

5.2. Characterization of water leachable fractions in soils samples and dusts

5.2.1. Sources of water soluble Ca and Sr in soils

The potential sources of water soluble Ca and Sr in soils include precipitation, bulk soluble background dust, gypsum dust from White Sands, and minerals in the soils (Figure 9). Compared to other sources, mineral dissolution originally sourced from bedrock was assumed to be slow to be critical in releasing ions to soils and low in concentrations (Francis *et al.*,1964). Rain or snow samples were not collected, but $^{87}Sr/^{86}Sr$ ratios in precipitation were reported to be between 0.7089-0.7092, with a Ca/Sr ratio greater than 0.36 at a site near Las Cruces, 160 km

away from White Mountains (Capo and Chadwick 1999). Elemental chemistry data for precipitation was downloaded from the National Trends Network (NTN) in the National Atmospheric Deposition Program (NADP). Data from 2011-2015 in Mayhill, New Mexico (station NM08, 65 km away, also a highland site with similar precipitation regimes) was aggregated and the loadings of dissolved calcium and sulfate through precipitation were estimated to be at 196 mg/m^2/year and 284 mg/m^2/year, respectively.

The gypsiferous samples collected at White Sands consisted nearly completely of Ca and SO_4 in the form of soluble gypsum (Table 3; Figure 4E). Due to the absence of non-soluble precipitates in White Sands samples after being dissolved and filtered, we assumed that water leachates and bulk sands had the same Sr isotopes and Ca/Sr ratios. White Sands gypsum samples (excluding the mixed Lake Lucero sediments) had $^{87}Sr/^{86}Sr$ ratios of 0.7078±0.0001 (n=9) and Ca/Sr ratios of 0.61 mol/mmol (Table 3; Figure 5).

We weighed the dust collected at the dust collector for two years, and based on the dimension of the pan, dust fell on the study site approximately at the rate 9.2 g/m^2/year. This is relatively low compared to dust fall in the region possibly due to orographic effects or trapping of dust in pines (Perez 2008; Rivas 2014). Of the bulk dust, only 6.6 wt% were water soluble, dominated by dissolved Ca (11 g/kg dust), Na (10 g/kg dust), K (8 g/kg dust), Cl (21 g/kg dust) and SO_4 (15 g/kg dust) (Table 3; Figure 7; Appendix C). In addition, trace amounts of water soluble Al, Fe, Mg, Mn, and F were present with concentrations under 1 g/kg dust. The $^{87}Sr/^{86}Sr$ ratio of dust leachate was 0.7081, and the Ca/Sr ratio was 0.35 mol/mmol (Figure 5). Aggregated dust leachate samples contained all atmospheric end members (rain, background, and White Sands gypsum). Precipitation was observed in the bottom of dust collector pans. Based on rainfall fluxes discussed above, contributions of rain to the water soluble portion of the dust

deposited in physical traps were estimated to be significant, approximately 66% for calcium and 67% for sulfate (Figure 9). Consistent with this, the Ca/Sr ratio in dust leachate was 0.35 mol/mmol, very close to rain water signature in literature (Capo and Chadwick 1999). White *et al.* (2015) studied elemental fluxes of dust ($PM_{2.5}$) less than 1km away from study sites where dust collectors were assembled, and reported that gypsum particles contributed approximately 40% of the calcium of the bulk dust signal. However, this study suggested that gypsum contribution by wt% was much lower than that for bulk dust. Indeed, the Sr isotopic ratio of the leachate dust at our study area was 0.7081, although the Sr isotope ratio in leachate samples near Las Cruces (100 km away and not receiving White Sands dust) was reported to be 0.7090±0.00001 (n=4) (Table 2; Capo and Chadwick 1999), very similar to precipitation signature.

5.2.2. Characterization of Salt Sources in soils

Gypsum or other salts were not detected in any bulk soil samples by XRD (Figure 4). This was consistent with the extremely low concentrations of soluble ions observed in soil leachates (Table 3; Figure 6; Figure 9). The dominant ions were Ca and SO_4, consistent with the chemistry of rain and dust leachates (Table 3; Figure 6). In all sites, total concentrations of soluble ions tended to increase down profile except for shallower soils at sites C and D (Table 3; Figure 7). These high values at soil surface may be due to biological and salt crusts that are common in the study region (Neher *et al.,* 2009). Increases of salinity down profile were largely attributed to calcium and sulfate near bedrock-soil interface, probably due to the presence of low permeability bedrock (Table 3; Figure 7). The same Ca/Sr trend in soil leachates was observed for all four sites, independent of the bedrock lithology, suggesting common atmospheric source(s) for Ca and Sr. Indeed, mineral dissolution as a source of soluble ions is minimal although shown to be a

possible input (Miller *et al.*, 2014.) Similarly, the $^{87}Sr/^{86}Sr$ of all soil leachates fell within those of two end-members (0.7078, White Sands gypsum, and 0.7081, water soluble fraction of the dust) except for A05, with a ratio of 0.7083. This also indicated that Lake Lucero sediments with dramatically different $^{87}Sr/^{86}Sr$ (0.7087) and the Ca/Sr ratios (2.45 mol/mmol), were not an important contributor of soluble Ca and Sr in soils (Table 3; Figure 5). Thus, the majority, if not all, of the water-soluble Ca and Sr in soils can be explained by the two atmospheric end members.

The $^{87}Sr/^{86}Sr$ ratio of precipitation was isotopically heavier than all dust and soil leachate samples in the system (0.7089-0.7092) (Capo and Chadwick, 1999), and precipitation contributed more calcium and strontium to the system than dust (Figure 9). Because all samples had $^{87}Sr/^{86}Sr$ far below the rain's signature, the rain was likely not contributing large amounts of Sr, and likely had a higher Ca/Sr than the minimum regional rainwater ratio of 0.36 (Capo and Chadwick, 1999).

In the soil leachates, Ca/Sr ratios decreased down profile at all sites (Table 3), possibly because of precipitation of secondary calcite in the profile and/or biological activity. The Ca/Sr ratio of most soil leachates fell between 0.23 and 0.61 mol/mmol, except for A00, A05, A10, B00, and D00, all samples near ground surface where soil organic carbon was high and biological activity was the highest, thus leading to possible biota alterations (Table 2; Figure 5).

White Sands gypsum contained little K or Na, so the existence of these two elements in soil leachates indicated inputs from different sources, likely rain or/and background dust (Table 3). Due to strong mobility and selective uptake by biota, these elements were transported at different rates throughout the soil profile (Adler *et al.*, 2009), and the relative inputs of gypsum, dust, and precipitation were not quantified using these elements as signatures.

A box model was used to estimate the fluxes of soluble Ca and Sr and their overall residence times within the critical zone (Figure 9). The total input of soluble calcium and sulfate into soil profiles measured over the study period was 296 mg/m^2/yr, and 425mg/m^2/yr, respectively. Flux inputs were calculated using the following formula:

$$Total\ flux\ C\ or\ SO_4\ mg/m^2/y = Precipitation_c * Precipitation_v + \frac{Dust_c * Dust_m}{Dust_a}$$

Where c = concentration of the element (either sulfate or calcium) in precipitation or dust sample, v = the volume of precipitation per year for a given geographic area m^2, m = the mass of dust flux per year, and a = the area of the dust pan (Table 3; Appendix C; Climate Data 2016). The concentration of elements in precipitation was estimated using the NADP NTN NM08 site in Mayhill, NM, and volume was estimated using climate data means over the last five years (Climate Data 2016). Dust mass flux was measured as a mean from all collectors, and area for dust pan was measured to be 0.135 m^2, which was converted to total flux per square meter per year (Appendix C). The average amount of soluble calcium and sulfate in the profile among four sites, assuming a depth of 0.5m, was estimated to be 39 g/m^2 and 71 g/m^2, respectively. This was calculated by estimating the mean concentration of the element of interest through all profiles and multiplying by soil kg/m^3, assuming that soil density is ~2 g/cm^3. Therefore, the residence time of Ca in the profiles was estimated to be 65 years, and the residence time of SO_4 in the profiles was estimated to be 83 years.

5.3. Uptake of calcium by vegetation

5.3.1. Source of Ca for all plants

Despite the variation in bedrock and soil $^{87}Sr/^{86}Sr$ signatures from 0.7072 to 0.7108, plant samples had a narrow range of Sr isotope ratios, from 0.7077 to 0.7082 in all cases except for the grass at site D (0.7090) (Table 2; Table 4). Additionally, Ca/Sr ratios in plants were also clustered based on plant type, regardless of bedrock. For instance, the Ca/Sr ratios of all plants at site A were scattered at 0.33±0.20 mol/mmol (Table 4). In contrast, the Ca/Sr ratios of all grasses among four sites were 0.25±0.04 mol/mmol (Table 4). Therefore, most of calcium and strontium taken up by plants were atmospherically derived, just like the water leachable fraction of the soils as previously discussed. Indeed, the soil leachates had $^{87}Sr/^{86}Sr$ ratio between 0.7078 and 0.7081, similar to all plant sample ratios. This is logical as water soluble nutrients are often considered as biologically available (Gosz and Moore 1989.) Interestingly, plant $^{87}Sr/^{86}Sr$ ratios of plants in the Sangre de Cristo Mountain range to the north are higher than those observed in this study, indicating a unique signal (White Sands) having a significant effect on Ca and Sr signatures (Gosz and Moore 1989). If water soluble fraction of the dust had relatively low Ca/Sr ratios (<0.1), the signature was likely less than all plant Ca/Sr values, constrained to 0.11-1.39 (Figure 5d). The Ca/Sr ratios of plant samples, however, were compared to soil leachates considering plant selective nutrient content and variance in plant root depth (Adler *et al.*, 2009.)

5.3.2. Variance in sites and plant type

All Ca/Sr ratios measured on plant samples were below 0.55mol/mmol, with the majority below 0.35 mol/mmol (Table 3). These were well below Ca/Sr ratios of the two end members, dust and precipitation, but fell within the Ca/Sr ratios of the soil leachates. The Ca/Sr ratios of

pine samples were generally the lowest of all plant species, (0.11-0.16, with an outlier BP1 of 0.30 mol/mmol, n = 4) (Table 4; Figure 7). The root depth of pines was generally the largest of all plant types. Thus, it was reasonable to conclude that nutrients such as Ca were taken up by pines from deeper soils, near soil-bedrock interface, where Ca/Sr ratios of the soil leachates were the lowest of all. In addition, $^{87}Sr/^{86}Sr$ ratios of pines were also among the lowest of all species, similar to those of the deepest soil leachates.

The Ca/Sr ratios in shrubs were higher than those in pines and varied more among sites, ranging from 0.25-0.55 mol/mmol (Table 3; Figure 5D). Shrubs probably had shallower roots than pines, and thus received nutrients at mid-soil layers, where Ca/Sr ratios of soil leachates were higher than those at depths. Different from pines, shrubs had large variations in both Ca/Sr and $^{87}Sr/^{86}Sr$ ratios (0.7077-0.7081), probably due to the different types of shrubs that were visually observed at each site and thus sampled (Figure 2).

The root depth of the grass was the shallowest of all plants, and the Ca/Sr ratios varied from 0.21-0.29 mol/mmol in grass samples, much higher than those observed in leachates of shallow soils. Grass samples had the most variable $^{87}Sr/^{86}Sr$ ratio between 0.7079 and 0.7090, always equal to or higher than the $^{87}Sr/^{86}Sr$ ratios of other plants at the same site (Table 4; Figure 5C). The variation in elemental ratios and isotopic ratios suggested that the calcium and strontium in grasses might not be sourced from soil leachates, but instead dependent on short-term rain or dust deposition, as the grasses were not perennial and would be more susceptible to seasonal variation in water and nutrient source and chemistry. The grass samples therefore demonstrated the spatiotemporal variability observed in atmospheric inputs, as they harvested calcium and strontium from recent deposition events. Alternatively, Ca/Sr ratios of grass samples did not

follow the depth trends of shrubs and pines, possibly because grasses fractionate these two elements during uptake (Figure 5D).

Interestingly, concentrations of other elements Fe, Na, Mn, and Mg in leaves of these plants varied more between sites than between plant types at sites (Table 4). For example, site B had sum of these elements at 1.2±0.5 wt%, significantly higher than both site A (mean 0.6±0.2 wt%) and site C (mean 0.3±0.2 wt%). This may be due to the extensive vegetation cover over site B by pine that trapped dust, while sites A and C were more chemically similar over more grassy areas.

The average plant reserves of calcium over sample sites were estimated to be 143 g/m^2 for grass, 1860 g/m^2 for pines, 1162 g/m^2 for shrubs, and 614 g/m^2 for cacti across all sites. This was calculated using the following formula:

$$\text{Mg Ca}/m^2 \text{ soil} = Ca_p (d_p * v_p)$$

Where Ca_p is the concentration of calcium per kilogram of plants (data reported in Table 3); d_p is the density of plants (assumed to be $0.95 g/cm^3$ for all plants); and v_p is the volume that plants take up per square foot of soil (Table 4; Haga *et al.*, 2017). The volume was calculated using visual assumptions observed at each site that grass is ~0.05m tall and covers 80% of the area of the site, that pines are ~2m tall and cover 10% of the area of the site, shrubs were ~1m tall and covered 10% of the area of the site, and cacti were ~0.40m tall and covered 5% of the area of the site (Figure 2). Based on the water leachate fluxes of for Ca (296 $mg/m^2/yr$) and the amount of soluble Ca in soils ($39 g/m^2$ for a 0.5m profile), I have concluded that Ca was not a limiting nutrient, even in the most weathering resistant sandstone at Site D.

6. CONCLUSIONS

In this study we have characterized the fluxes and mobility of gypsum dust in soil profiles by evaluating 1) bulk soil chemistry controls, 2) sources of water leachable elements in soil profiles, and 3) plant Ca sources. This analysis was performed in a study area previously confirmed to receive the White Sands gypsum in dry and wet deposition in addition to regional dust (Figure 1; White *et al.,* 2015). Bedrock weathering dominated bulk chemistry over carbonate profiles. Minimal Ca input from bedrock was observed in profiles over igneous and siliciclastic substrates, so bulk dust addition of Ca was detected. Gypsum was not detectable in bulk soils in dust or soils during the two-year period of dust collection, suggesting its fast dissolution in soils and higher mobility Indeed, dust water leachable ion concentrations were less than 10 wt% and profile concentrations of soluble elements were much lower.

The water leachable fraction component of the soil was largely constrained by atmospheric end members of White Sands gypsum and dust leachable samples and did not vary based on bedrock, indicating that bedrock mineral dissolution was minimal. Calcium and sulfate were the dominant species in the soil leachates, and $^{87}Sr/^{86}Sr$ isotopes indicated White Sands was a significant contributor to soluble Ca and Sr at the sites. Ca and Sr moved differently through profiles, likely due to biological activity or secondary calcite precipitation, yielding Ca/Sr values lower than both end members. Ca and Sr used in plants was also largely constrained to water leachable fractions of atmospheric inputs, and signature of calcium and strontium were closer within plant types than between sites. Concentrations of elements other than calcium and strontium in plants were more dependent on site.

7. FURTHER CONSIDERATIONS AND FUTURE WORK

Volumes and chemical characteristics of gypsum and other aerosol sources reaching White Mountain vary in time and space, especially in the case of White Sands, which episodically emits based on large drying and wetting events (Allmendinger 1973; White *et al.,* 2015). Additionally, the impact of dust kinetics and trapping vary from vegetation, geomorphology, meteorological patterns, and time of year (Knippertz and Stuut 2014). Dust collection was over 2 years, and volume collected was still small, limiting analyses run and measurements of dust spatiotemporal heterogeneity. The dust was collected and aggregated over different time periods. Different times of the year contribute different proportions and volumes of dust and salts from gypsum, rain, and background dust (White *et al.,* 2015). In order to collect a more representative dust sample, it is recommended to collect multiple dust samples for much longer time periods.

Precipitation and chemistry data from NADP NTN NM08 site in Mayhill, New Mexico suggest that rain in this area contributes significant amounts of aqueous calcium, strontium, and sulfate (Figure 9). Samples from snow and rain should be collected to quantify this end member. Dust water leachable samples contain dust, rain, and organic matter, all which may contain trace amounts of Ca, Sr, and SO_4. Placement of a dust collector in Bosque del Apache, the Organ Mountains, or the San Andres Mountains may better quantify background dust signature.

Plant chemistry may vary between different parts of the plant (Neher *et al.,*2009.) Only leaves were considered in this study, and more quantitative species designation and sampling of stems, wood cores, and roots of the plant would help better understand the dynamics of plant nutrient mobility in this system.

Table 1: Characteristics of study sites and samples

Site	Latitude (°N)	Longitude (°W)	Lithology	Formation	~Age (MYA)	Notes
Soil profiles:						
A	33.472	105.536	Limestone	Artesia	265	Ridge top, one dust collector, plants collected include Grass, pine, shrub
B	33.461	105.573	Diorite	N/A	15	Steep slope, vegetated, west-facing, plants collected include cactus, grass, 2 pines, shrub
C	33.469	105.515	Limestone/Dolostone	San Andres	275	Ridge top, with one dust collector, plant samples collected include grass, pine, 2 shrubs
D	33.448	105.661	Sand/Siltstone	Mesa Verde	100	Shallow slope, low amounts of vegetation, west-facing, plant samples collected include grass, pine, shrub
White Sands samples:						
WS1	32.698	106.451	Selenite/Gypsum	Yeso	260	Lake Lucero sediments
WS2	32.887	106.123	Gypsum	Yeso	260	Parabolic dune and interdune
WS3	32.886	106.260	Gypsum	Yeso	260	Barchan dune and interdune
WS4	32.871	106.280	Gypsum, Dolomite	Yeso	260	Ridge over Alkali Flats
WS5	32.871	106.271	Gypsum	Yeso	260	Ridge over Alkali Flats
WS6	32.871	106.279	Gypsum	Yeso	260	Ridge over Alkali Flats
WS7	32.868	106.432	Gypsum	Yeso	260	Coarse flats material
Dust Samples*: mixed aggregate of total dust gathered from sites A and C over 2 years. See appendix E for details.						

Table 2: Bulk Soil and Rock Chemistry

Sample	Depth	Al_2O_3	CaO	Fe_2O_3	K_2O	MgO	MnO	Na_2O	PO_5	TiO_2	Ba	Sr	Zr	Ca/Sr	Total	TOC	Calcite/ Dolomite*	$^{87}Sr/^{86}Sr$
	cm	%	%	%	%	%	%	%	%	%	ppm	ppm	ppm	mol/mmol	%	%	%	
A00	0-5	14.2	5.7	4.26	3.16	1.25	0.08	2.12	0.23	0.77	866	272	281	0.32	4.0	3.7	2.8	0.7080
A05	5-10	13.2	6.3	4.05	2.80	1.16	0.07	1.79	0.13	0.72	782	275	342	0.36	3.9	3.2	5.6	0.7088
A10	10-15	13.8	7.2	4.21	2.89	1.22	0.07	1.93	0.20	0.75	848	276	308	0.41	3.9	3.1	6.4	0.7077
A15	15-20	14.1	8.2	4.35	3.02	1.26	0.08	1.94	0.17	0.77	878	295	281	0.43	3.7	3.0	6.2	0.7087
A20	20-25	13.5	7.3	4.14	2.86	1.17	0.07	1.79	0.17	0.74	815	284	352	0.40	3.7	2.8	7.3	0.7087
A25	25-30	14.0	9.9	4.18	3.06	1.18	0.07	2.08	0.22	0.74	885	295	331	0.52	4.0	2.8	9.9	0.7087
A30	30-35	13.4	14.0	3.91	2.96	1.09	0.06	1.91	0.23	0.71	822	303	345	0.72	4.8	2.9	15.4	0.7086
A35	35-40	14.4	24.0	4.68	3.82	1.35	0.08	2.46	0.33	0.84	1743	466	379	0.80	5.6	2.8	23.0	0.7084
A40	40-50	11.5	21.3	3.35	2.46	1.02	0.05	1.59	0.22	0.58	747	319	260	1.04	5.9	2.4	29.4	0.7084
A50	50-60	9.2	31.4	2.53	2.01	0.86	0.04	1.51	0.16	0.45	927	373	175	1.32	7.5	1.8	48.0	0.7079
A:bedrock	65	2.9	51.4	0.71	0.50	0.52	0.01	0.26	0.11	0.10	369	301	94	2.67	11.7	0.5	93.0	0.7083
B00	0-5	16.4	2.3	6.04	4.43	1.20	0.14	3.17	0.21	1.16	1703	422	473	0.08	4.0	4.3		0.7080
B05	5-10	16.4	2.5	5.23	3.56	1.14	0.11	2.48	0.15	0.95	903	321	382	0.12	3.4	3.2		0.7077
B10	10-15	16.4	2.0	5.18	3.56	1.09	0.09	2.57	0.07	0.92	915	322	338	0.10	2.5	2.5		0.7089
B15	15-20	17.1	2.3	5.31	3.72	1.20	0.09	2.66	0.13	0.95	950	330	401	0.11	2.4	2.4		0.7075
B20	20-35	17.0	1.9	5.20	3.62	1.13	0.09	2.63	0.09	0.94	889	310	278	0.10	2.0	2.2		0.7073
B35	35-40	18.3	2.5	5.62	3.87	1.31	0.10	2.82	0.07	0.95	1041	348	371	0.11	1.9	1.9		0.7070
B:bedrock	45	16.3	2.1	4.32	4.32	0.75	0.13	3.60	0.22	0.84	1104	238	486	0.14	1.5	1.6		0.7072
C00	0-5	15.0	7.6	4.94	3.20	1.28	0.09	2.43	0.26	0.85	892	351	329	0.34	3.4	2.5	6.8*	0.7075
C05	5-10	14.1	6.2	5.03	2.83	1.36	0.09	2.00	0.24	0.86	781	326	354	0.30	3.7	3.1	4.3*	0.7073
C10	10-15	14.2	8.1	5.02	2.90	1.28	0.08	2.15	0.24	0.85	821	338	342	0.38	3.1	2.0	8.6*	0.7078
C15	15-20	13.4	6.5	4.64	2.68	1.24	0.08	2.04	0.19	0.77	762	305	293	0.33	3.4	2.6	5.9*	0.7074
C20	20-25	14.4	7.5	5.04	2.90	1.32	0.09	2.14	0.23	0.88	819	332	359	0.35	3.2	2.2	7.4*	0.7074
C25	25-30	14.1	7.9	4.84	2.89	1.27	0.08	2.14	0.18	0.83	807	326	336	0.38	3.1	2.0	8.0*	0.7074
C30	30-35	14.1	8.3	4.80	2.82	1.26	0.08	2.10	0.17	0.82	814	335	396	0.39	3.1	1.9	8.9*	0.7075
C35	35-40	12.7	8.7	4.69	4.42	1.24	0.08	3.30	0.49	0.79	782	353	302	0.38	2.8	1.6	9.3*	0.7074
C40	40-45	13.0	9.5	4.94	2.87	1.26	0.08	2.03	0.21	0.83	817	365	377	0.41	3.0	1.6	10.8*	0.7076
C45	45-50	13.8	9.4	4.80	2.82	1.23	0.08	2.00	0.20	0.84	803	352	308	0.42	3.3	1.8	11.0*	0.7075
C:bedrock	55	14.2	8.6	3.95	3.49	0.91	0.08	2.44	0.27	0.73	784	262	475	0.51	2.7	0.1	20.1*	0.7100
D00	0-5	9.3	0.9	3.55	1.47	0.62	0.05	1.41	0.12	0.58	454	225	350	0.06	1.0	n.d.	n.d.	0.7103
D05	5-10	10.2	1.0	3.90	1.70	0.73	0.05	1.38	0.20	0.67	459	222	391	0.07	1.2	n.d.	n.d.	0.7108
D10	10-15	12.2	0.8	4.50	1.67	0.84	0.05	0.73	0.07	0.65	449	160	340	0.08	1.4	n.d.	n.d.	0.7107
D15	15-20	18.8	1.3	6.83	2.48	1.24	0.08	1.32	0.28	0.97	720	242	469	0.09	1.3	n.d.	n.d.	0.7112
D20	20-25	12.5	0.9	4.69	1.74	0.88	0.05	0.83	0.10	0.66	589	174	379	0.08	1.3	n.d.	n.d.	0.7112
D:bedrock	30	7.7	0.2	7.06	0.56	0.94	0.02	0.75	0.04	0.62	1227	101	562	0.03	0.2	n.d.	n.d.	0.7108
Dust	n.d.	n.d.	n.d.	n.d.	n.d.	n.d.	n.d.	n.d.	n.d.	n.d.	n.d.	n.d.	n.d.	n.d.	n.d.	36.4	n.d.	0.7087

Carbonate % was calculated by subtracting TOC% from total carbon % and converting carbon to calcite (100/12) or dolomite* (184/24) until carbon was

*Carbonate types at site C includes both dolomite and calcite identified in mineralogy analysis. Carbonates in sites A, B, and D are calcite.

† Calcium used in carbonates was subtracted from bulk calcium in soil. The remainder is calcium available for other minerals (e.g. plagioclase, gypsum.)

Table 3: Elemental chemistry and $^{87}Sr/^{86}Sr$ isotopes of soil and dust leachate samples

	pH	EC	Soil:Water	Al	Ca	K	Na	Sr	F	Cl	SO_4	NO_3	PO_4	$CaSO_{4*}$	$^{87}Sr/^{86}Sr$	Ca/Sr
		µS/cm	g/L	mg/kg	mg/kg	mg/kg	mg/kg	mg/kg	mg/kg	mg/kg	mg/kg	mg/kg	mg/kg	mg/kg		mol/mmol
A00	7.2	82	46.3	0.3	17.2	2.4	0	0	3.2	26.6	16.0	30.4	0.8	23	0.7080	1.40
A05	7.0	72	47.1	0.2	17.7	0.8	0	0.1	7.1	14.2	14.8	0	10.0	21	0.7083	0.64
A10	7.0	73	46.2	0.3	14.3	0.6	0	0	7.6	15.6	10.3	0	0.2	15	0.7080	0.64
A15	7.2	69	47.9	0.2	20.6	1.6	0	0.1	8.9	7.6	24.6	0	0.9	35	0.7080	0.43
A20	6.7	74	49.4	0.2	19.8	2.0	1.3	0.1	9.1	5.9	20.7	0	0.2	30	0.7080	0.40
A25	6.8	78	50.3	0.2	22.8	2.1	0.7	0.1	10.1	9.4	26.1	0.2	0.5	38	0.7079	0.36
A30	7.2	94	52.9	0.2	19.1	2.9	1.9	0.1	11.1	12.9	33.8	0	1.7	49	0.7080	0.35
A35	6.9	113	56.1	0.2	23.4	2.7	1.2	0.1	10.5	17.1	107.9	0.3	0.6	155	0.7080	0.36
A40	7.0	101	43.0	0.2	16.9	3.1	1.5	0.1	14.9	19.2	68.3	0	0.1	98	0.7079	0.33
A50	7.1	131	39.0	0.2	29.7	2.6	0	0.2	4.7	13.4	67.5	0	0.3	97	0.7080	0.27
B00	6.5	24	51.5	1.6	5.4	3.5	2.8	0	1.4	14.5	9.6	0	14.4	14	0.7080	1.22
B05	6.5	26	46.0	2.7	7.7	4.0	0	0	4.0	9.3	10.5	0	2.5	15	0.7080	0.38
B10	6.0	42	59.8	2.7	6.3	3.5	0	0	4.3	10.4	33.2	0.5	1.5	48	0.7080	0.35
B15	6.0	27	57.3	1.4	9.1	3.0	0	0.1	5.1	11.9	40.1	0	0.5	58	0.7079	0.28
B20	6.0	33	53.2	0.6	9.5	2.9	0.7	0.1	5.9	17.1	68.4	0	0.1	98	0.7079	0.27
B35	7.0	68	52.6	0.3	15.5	3.2	1.4	0.1	11.3	11.6	43.0	0	0.4	62	0.7079	0.25
C00	7.0	74	54.0	0.2	30.9	5.5	1.2	0.2	5.7	9.2	31.2	12.0	0.3	45	0.7079	0.33
C05	7.1	90	56.4	0.2	21.9	3.7	0	0.1	8.7	14.1	19.7	0.1	0.4	28	0.7079	0.50
C10	7.4	64	47.8	0.3	25.1	2.6	0	0.1	8.6	15.0	28.3	0	0.3	41	0.7079	0.43
C15	7.3	69	50.5	0.2	25.9	2.4	0	0.1	6.0	24.3	25.5	0	0.4	37	0.7080	0.51
C20	7.1	84	66.4	0.2	27.5	1.8	0	0.1	8.9	11.8	28.3	0.1	0.1	41	0.7079	0.43
C25	7.5	74	49.3	0.2	28.0	1.8	1.0	0.2	9.9	15.6	50.0	0	0.3	72	0.7078	0.37
C30	6.7	89	48.3	0.2	32.4	3.0	0.4	0.2	15.2	16.4	30.6	0	0	44	0.7078	0.32
C35	7.1	80	53.4	0.2	30.8	1.6	1.6	0.3	6.2	7.7	19.2	0	1.1	28	0.7078	0.26
C40	7.3	54	42.7	0.2	30.7	1.8	1.6	0.3	8.5	8.6	21.8	0	0.2	31	0.7078	0.24
C45	7.4	65	45.6	0.2	35.3	2.4	1.0	0.3	13.8	20.8	73.5	0	0.2	106	0.7078	0.23

Table 3: Elemental chemistry and $^{87}Sr/^{86}Sr$ isotopes of soil and dust leachate samples (continued)

	pH	EC	Soil:Water	Al	Ca	K	Na	Sr	F	Cl	SO_4	NO_3	PO_4	$CaSO_{4*}$	$^{87}Sr/^{86}Sr$	Ca/Sr
		µS/cm	g/L	mg/kg	mg/kg	mg/kg	mg/kg	mg/kg	mg/kg	mg/kg	mg/kg	mg/kg	mg/kg	mg/kg		mol/mmol
D00	6.1	181	138.7	3.6	149.8	76.0	22.7	0.3	2.0	27.5	4.9	35.0	0	7	0.7081	0.99
D05	6.4	23	132.7	6.5	49.1	24.6	14.6	0.3	3.9	5.5	13.4	0	0.1	19	0.7080	0.32
D10	6.5	24	129.7	6.3	50.4	23.1	18.6	0.4	3.2	8.0	22.8	0	0	33	0.7080	0.29
D15	6.5	28	145.3	4.8	61.0	25.4	22.2	0.4	3.6	4.6	26.8	0	0.3	39	0.7080	0.33
D20	6.5	29	144.0	4.4	72.7	27.5	22.8	0.6	3.3	10.0	31.2	0	0	45	0.7080	0.28
Dust (leachate)†	6.6	47200	34.8	73	10965	7980	10428	68	219	20943	15697	0	53	22612	0.7081	0.35
WS1	n.d.	654	0.5	202	330683	0	1616	296	1616	867	520810	8207	2352	750257	0.7087	2.45
WSD2	n.d.	661	0.6	n.d.	n.d.	n.d.	n.d.	n.d.	209	1233	509113	6404	0	733406	0.7078	n.d.
WSI2	n.d.	610	0.5	n.d.	n.d.	n.d.	n.d.	n.d.	150	699	458589	6688	0	660624	0.7078	n.d.
WSD3	n.d.	874	0.7	n.d.	n.d.	n.d.	n.d.	n.d.	171	592	433889	6166	0	625042	0.7078	n.d.
WSI3	n.d.	578	0.5	n.d.	n.d.	n.d.	n.d.	n.d.	160	604	354939	6111	0	511310	0.7078	n.d.
WSD4	n.d.	575	0.5	n.d.	n.d.	n.d.	n.d.	n.d.	200	709	580944	7835	0	836883	0.7078	n.d.
WSD4d	n.d.	608	0.5	n.d.	n.d.	n.d.	n.d.	n.d.	175	491	525214	5366	0	756601	0.7079	n.d.
WSD5	n.d.	653	0.6	n.d.	n.d.	n.d.	n.d.	n.d.	233	729	463080	7624	0	667093	0.7078	n.d.
WSD6	n.d.	722	0.6	n.d.	n.d.	n.d.	n.d.	n.d.	209	679	461608	7467	0	664973	0.7079	n.d.
WSD7	n.d.	6034	1.1	n.d.	n.d.	n.d.	n.d.	n.d.	210	2896	482951	7390	0	695718	0.7079	n.d.

* Gypsum mg/kg was converted using SO_4 levels translated to gypsum mass.

† Dust sample is an aggregate of all samples from site C (appendix E.) Dust samples contain rain water and background salt.

Table 4: Chemistry of Plant Samples

Sample	ID	Al	Ca	Fe	K	Mg	Mn	Sr	Ca/Sr	$^{87}Sr/^{86}Sr$
		ppm	ppm	ppm	ppm	ppm	ppm	ppm	mol/mmol	
Site A: Grass	AG	1143	3436	1278	2597	710	68	26	0.29	0.7082
Site A: Pine	AP	78	8632	78	5290	997	21	120	0.16	0.7077
Site A: Shrub	AS	62	11246	68	6634	1352	260	45	0.55	0.7078
Site B: Cactus	BC	31	32320	24	11542	7733	70	262	0.27	0.7077
Site B: Grass	BG	1331	5222	1408	5740	1086	85	56	0.21	0.7079
Site B: Pine 1	BP1	98	9348	98	11385	2604	121	67	0.30	0.7077
Site B: Pine 2	BP2	85	14491	88	4800	1281	38	229	0.14	0.7077
Site B: Shrub	BS	97	10950	114	10015	1539	321	80	0.30	0.7077
Site C: Grass	CG	118	2619	112	653	225	31	24	0.24	0.7080
Site C: Pine	CP	115	6689	80	4293	945	14	139	0.10	0.7079
Site C: Shrub 1	CS1	99	14512	71	2470	1402	74	68	0.47	0.7080
Site C: Shrub 2	CS2	47	6660	38	8453	937	94	58	0.25	0.7080
Site D: Grass	DG	n.d.	n.d.	n.d.	n.d.	n.d.	n.d.	n.d.	n.d.	0.7090
Site D: Pine	DP	n.d.	n.d.	n.d.	n.d.	n.d.	n.d.	n.d.	n.d.	0.7081
Site D: Shrub	DS	n.d.	n.d.	n.d.	n.d.	n.d.	n.d.	n.d.	n.d.	0.7081

*The first letter of plant ID indicates site; second letter plant type: G for grass, S for shrub, P for pine, C for cactus.

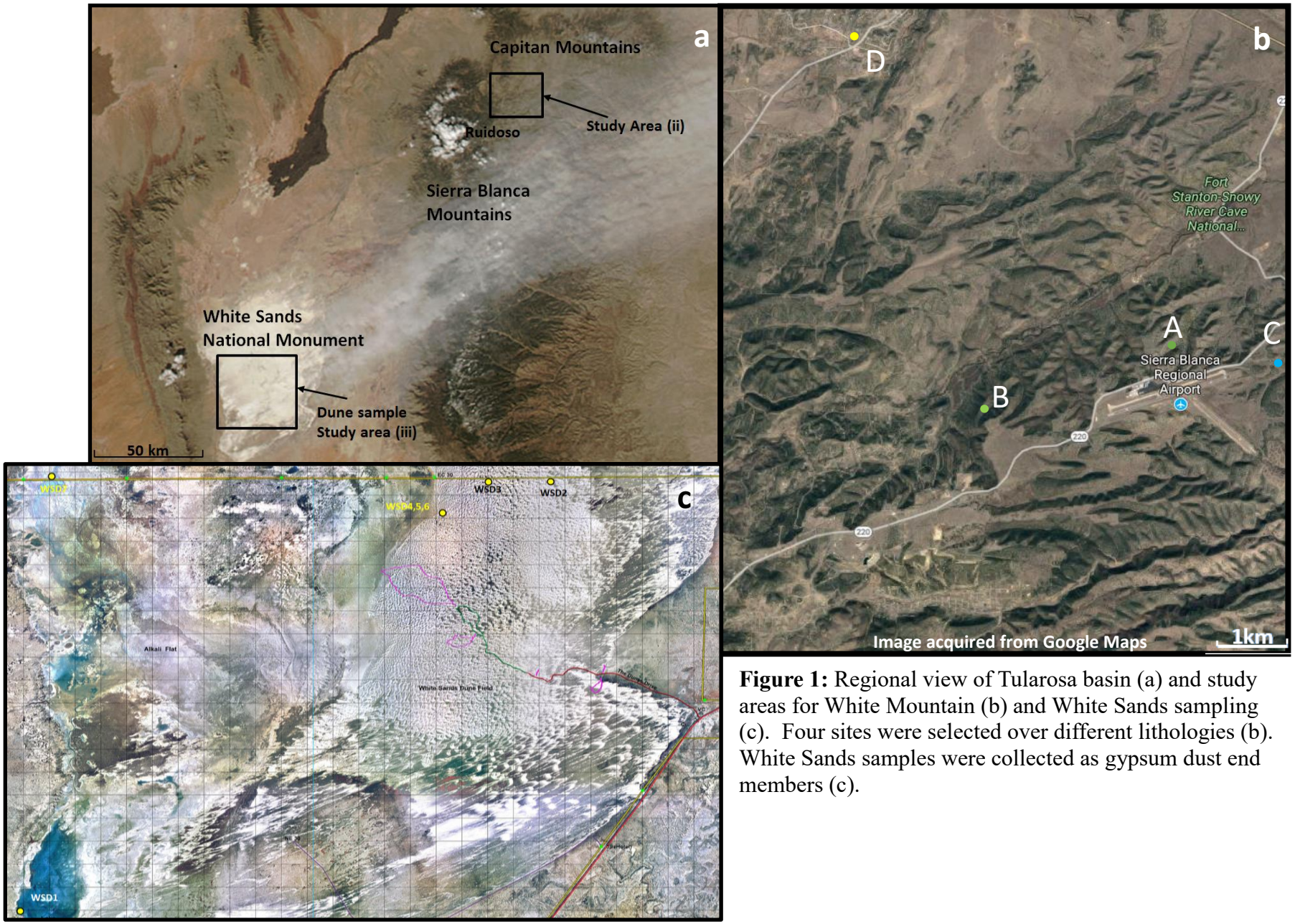

Figure 1: Regional view of Tularosa basin (a) and study areas for White Mountain (b) and White Sands sampling (c). Four sites were selected over different lithologies (b). White Sands samples were collected as gypsum dust end members (c).

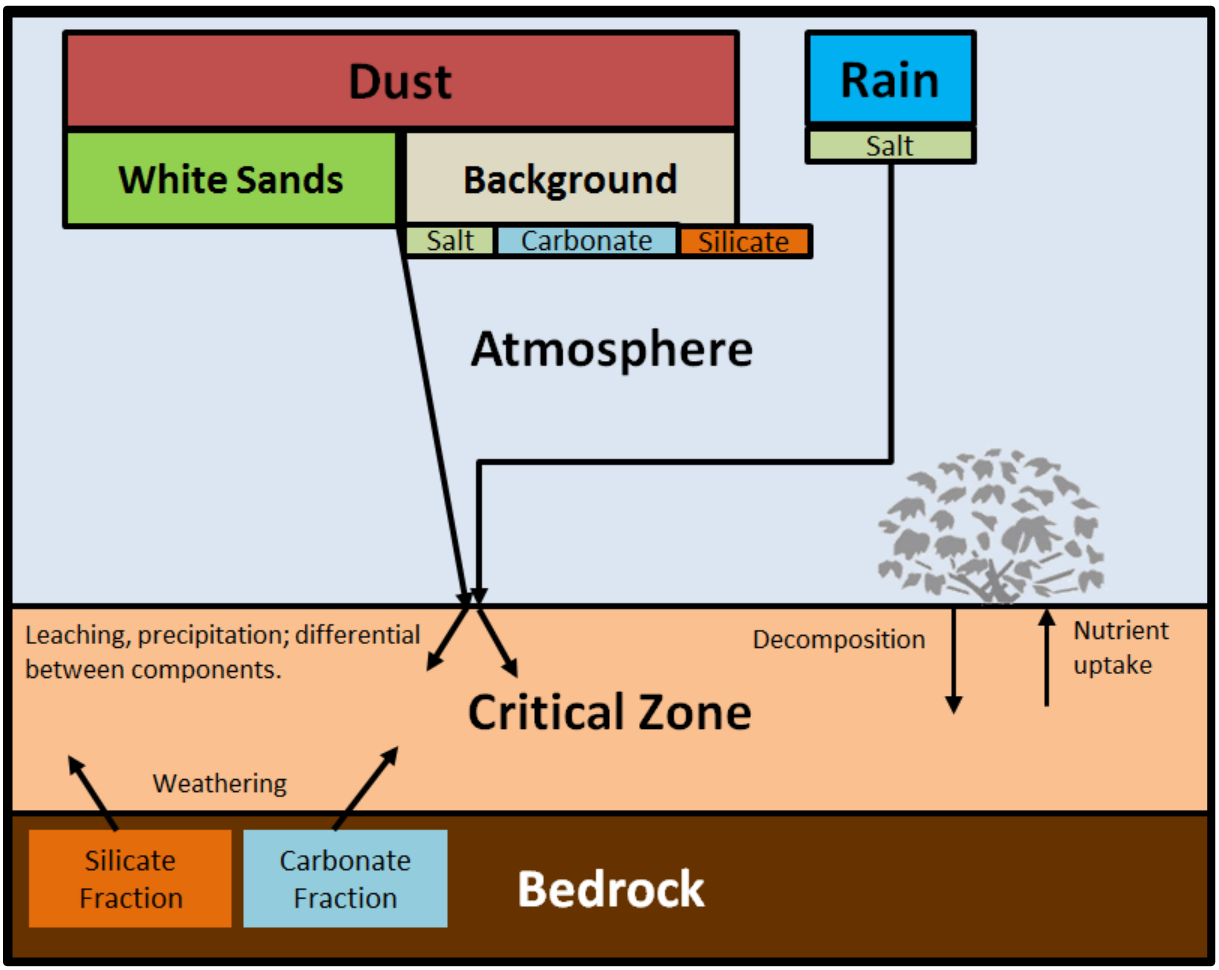

Figure 2: Inputs, outputs, and internal cycling within the critical zone. All potential end members are considered with their varying component mobility.

Figure 3: (A) dust collector at site A; (B) site C shrub; (C) site C pine.

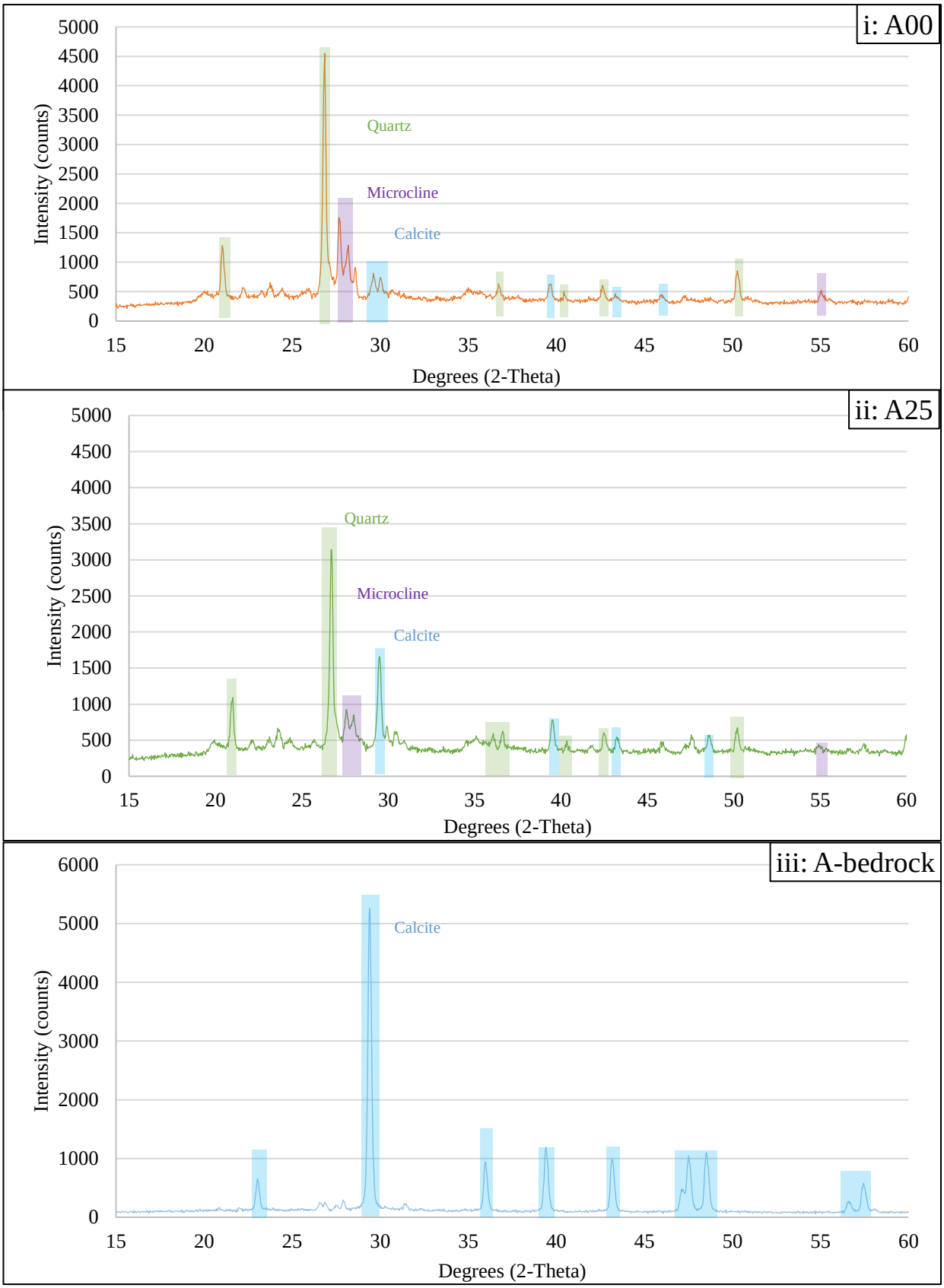

Figure 4a: Major minerals identified in soils and bedrock at site A: (i) A00; (ii) A25; (iii) A-bedrock.

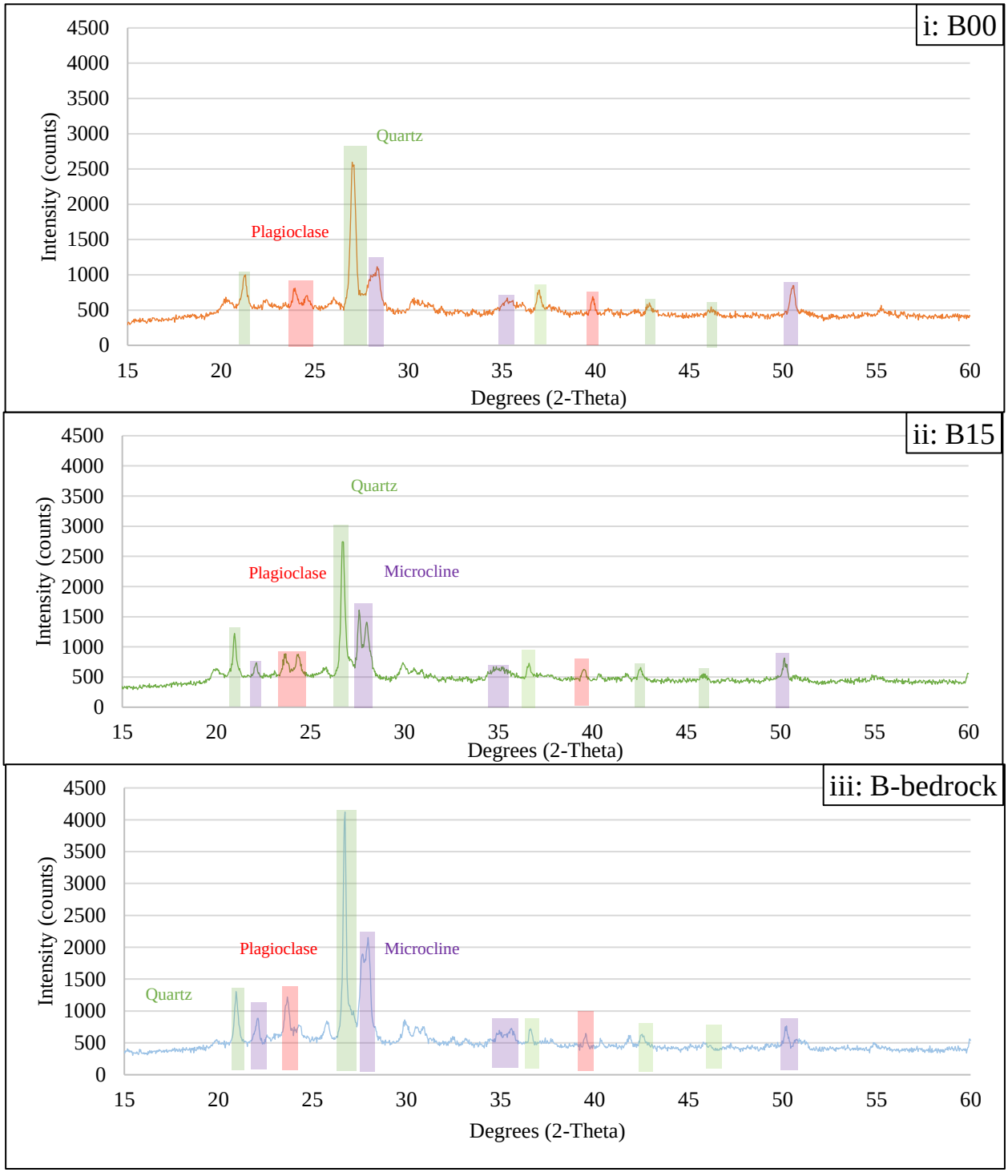

Figure 4b: Major minerals identified in soils and bedrock at site B: (i) B00; (ii) B15; (iii) B-bedrock.

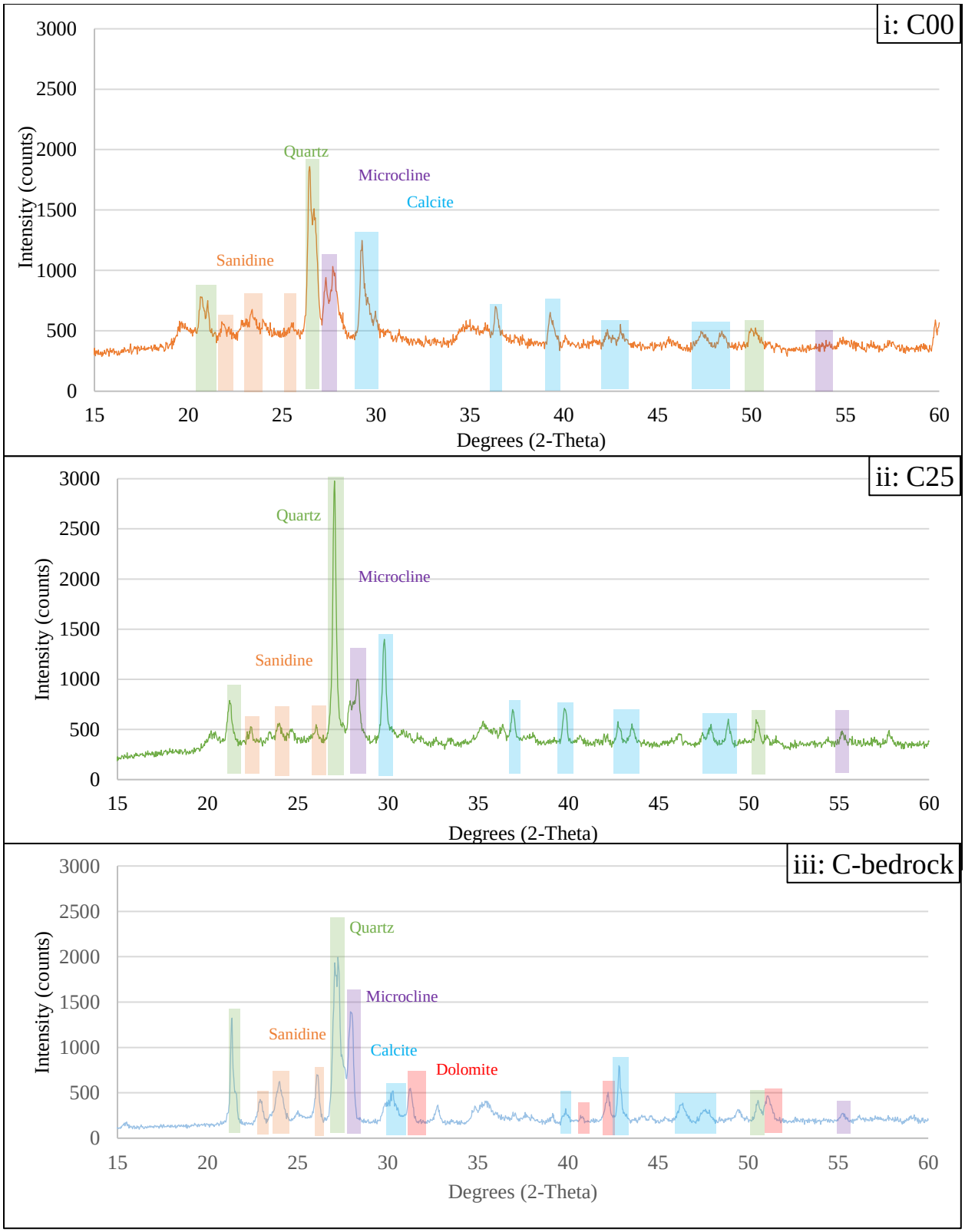

Figure 4c: Major minerals identified in soils and bedrock at site C: (i) C00; (ii) C25; (iii) C-bedrock.

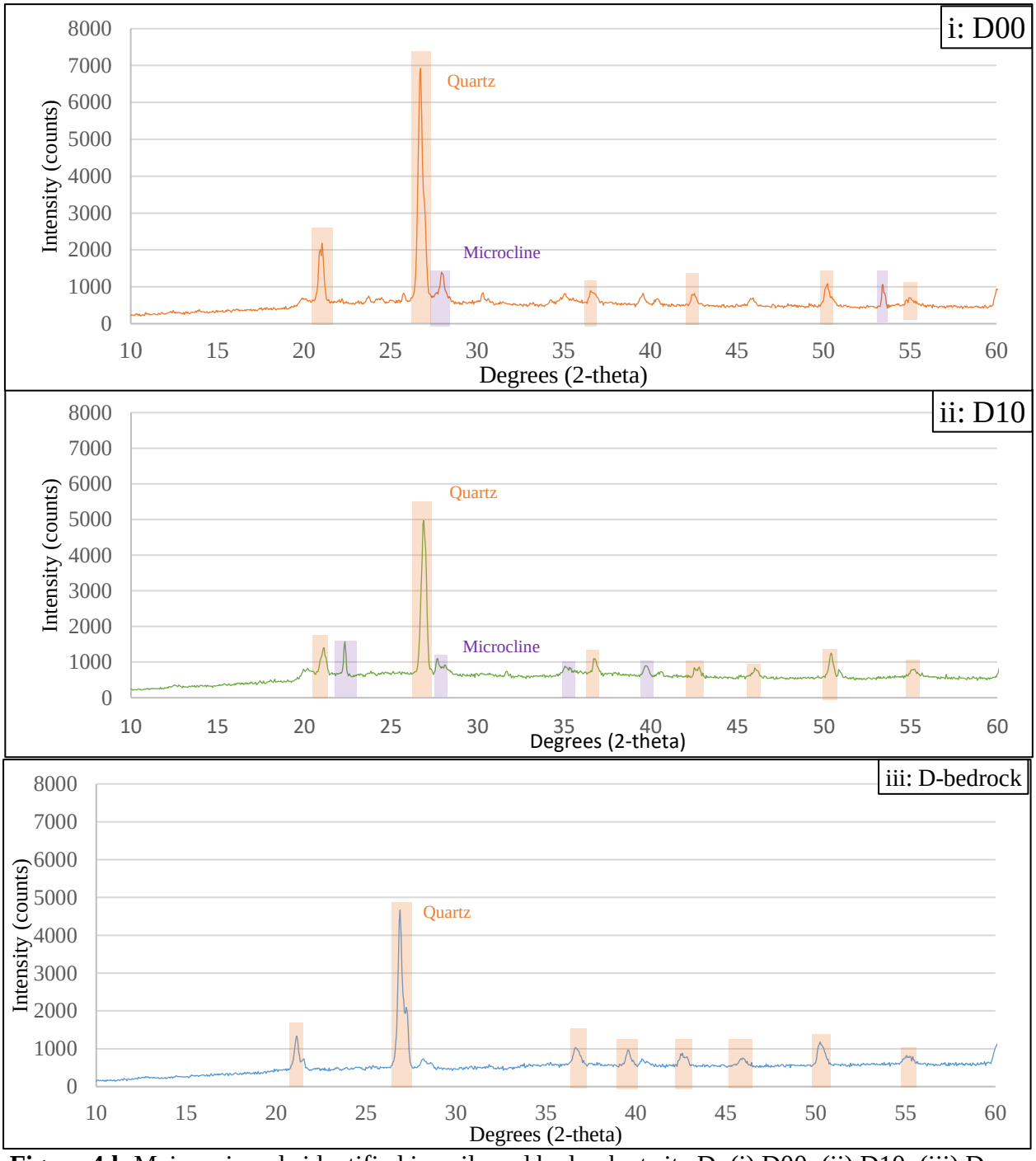

Figure 4d: Major minerals identified in soils and bedrock at site D: (i) D00; (ii) D10; (iii) D-bedrock.

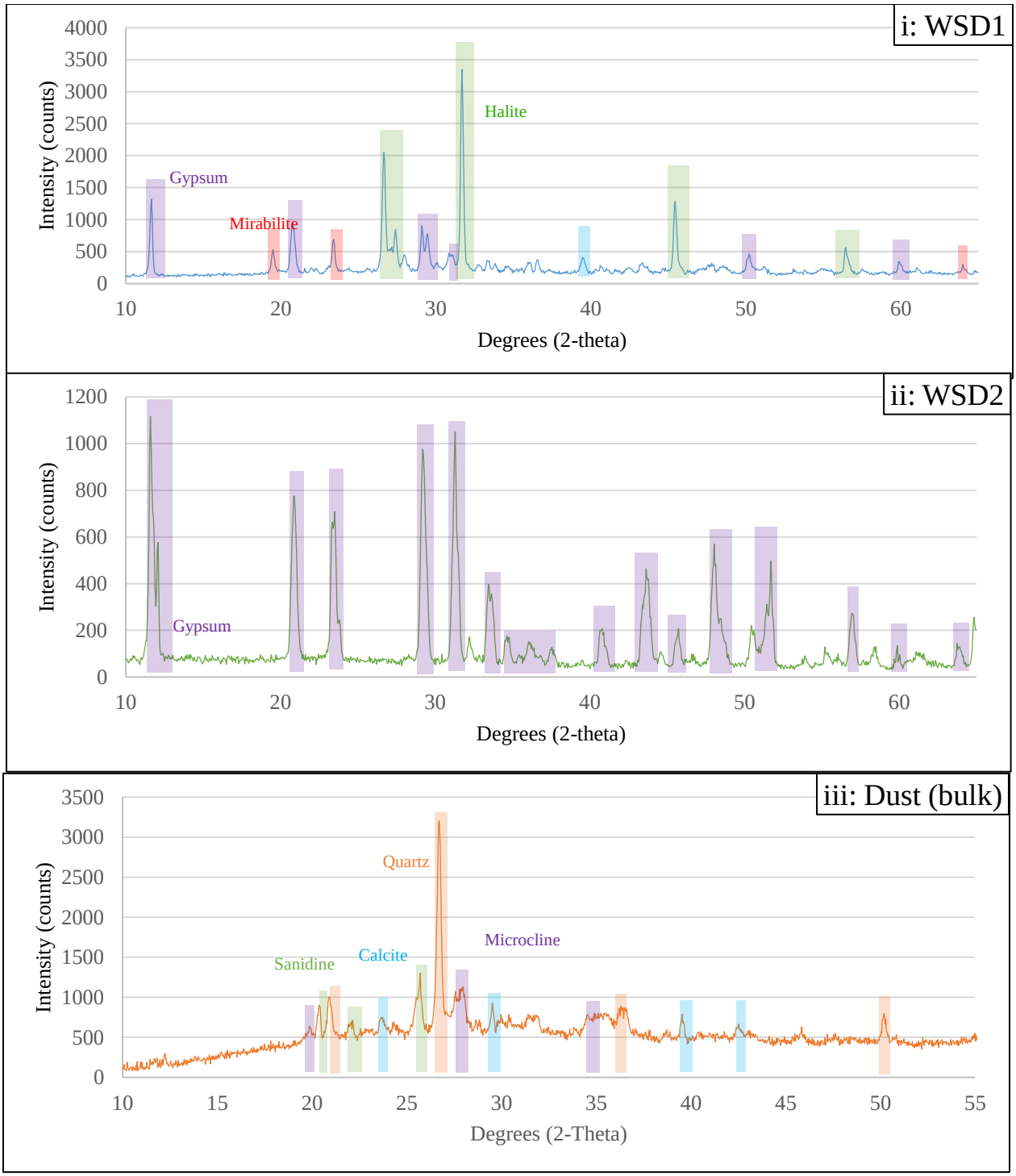

Figure 4e: Major minerals identified in dust and White Sands samples: (i) WSD1 (Lake Lucero sediments); (ii) WSD2 (parabolic dune crest); (iii) Dust (bulk.)

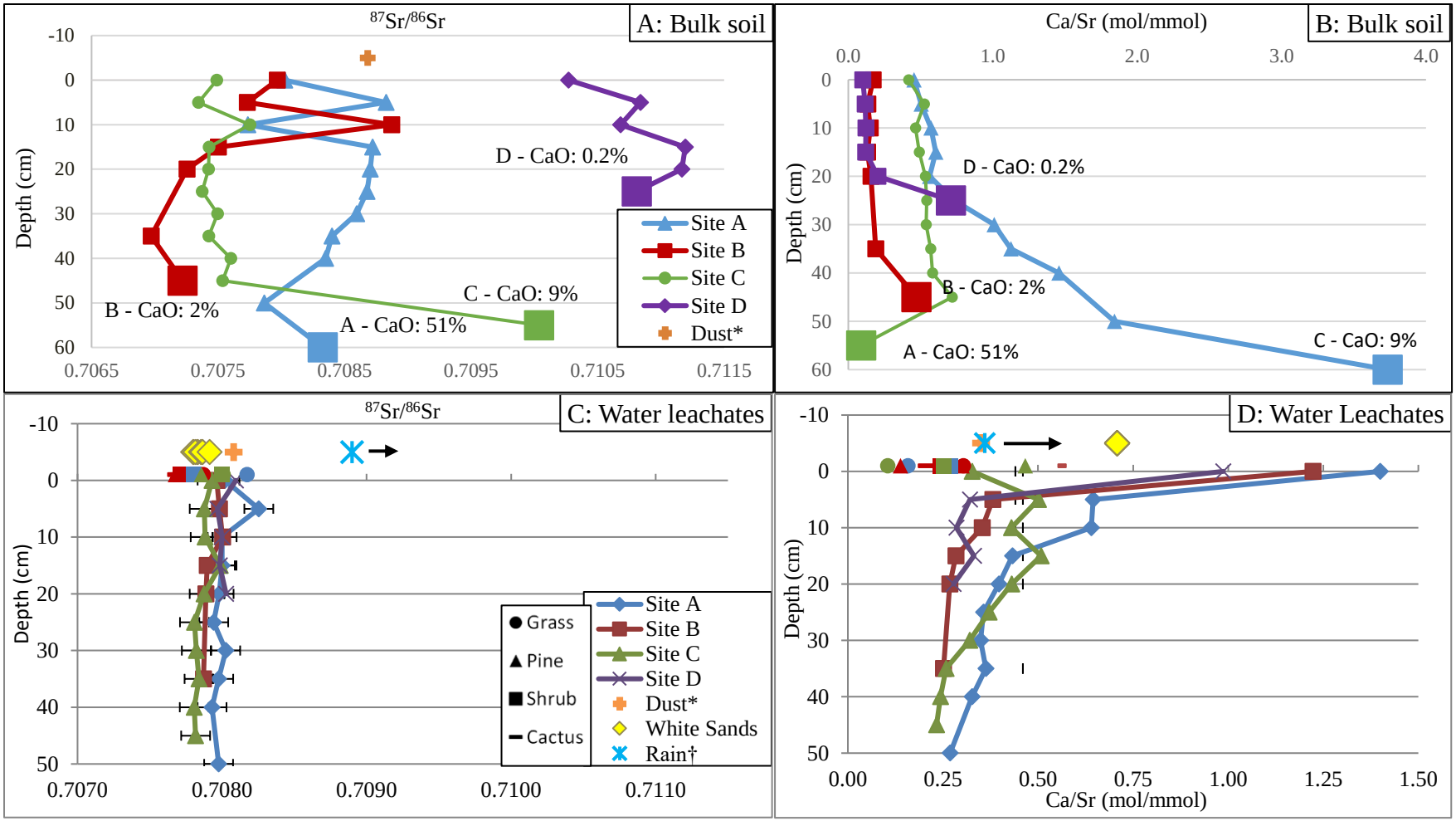

Figure 5: Variation of (A) $^{87}Sr/^{86}Sr$ in all bulk soil, rock, and dust samples as a function of depth, (B) $^{87}Sr/^{86}Sr$ in all water leachate and plant samples as a function of depth, (C) Ca/Sr in all bulk soil and rock samples as a function of depth, and (D) Ca/Sr in all water leachate and plant samples as a function of depth. The deepest sample in each weathering profile (labelled as squares) in 5a and 5c indicate bedrock, labeled in CaO wt%. Shapes of plant samples in 5b and 5d indicate type: grass (circles,) pines (triangles,) shrubs (squares,) and cacti (dashes.)

*Dust leachate contains some rain water.

† Rain data from Capo and Chadwick (1999) suggests minimum Ca/Sr ratio and regional $^{87}Sr/^{86}Sr$ ratios.

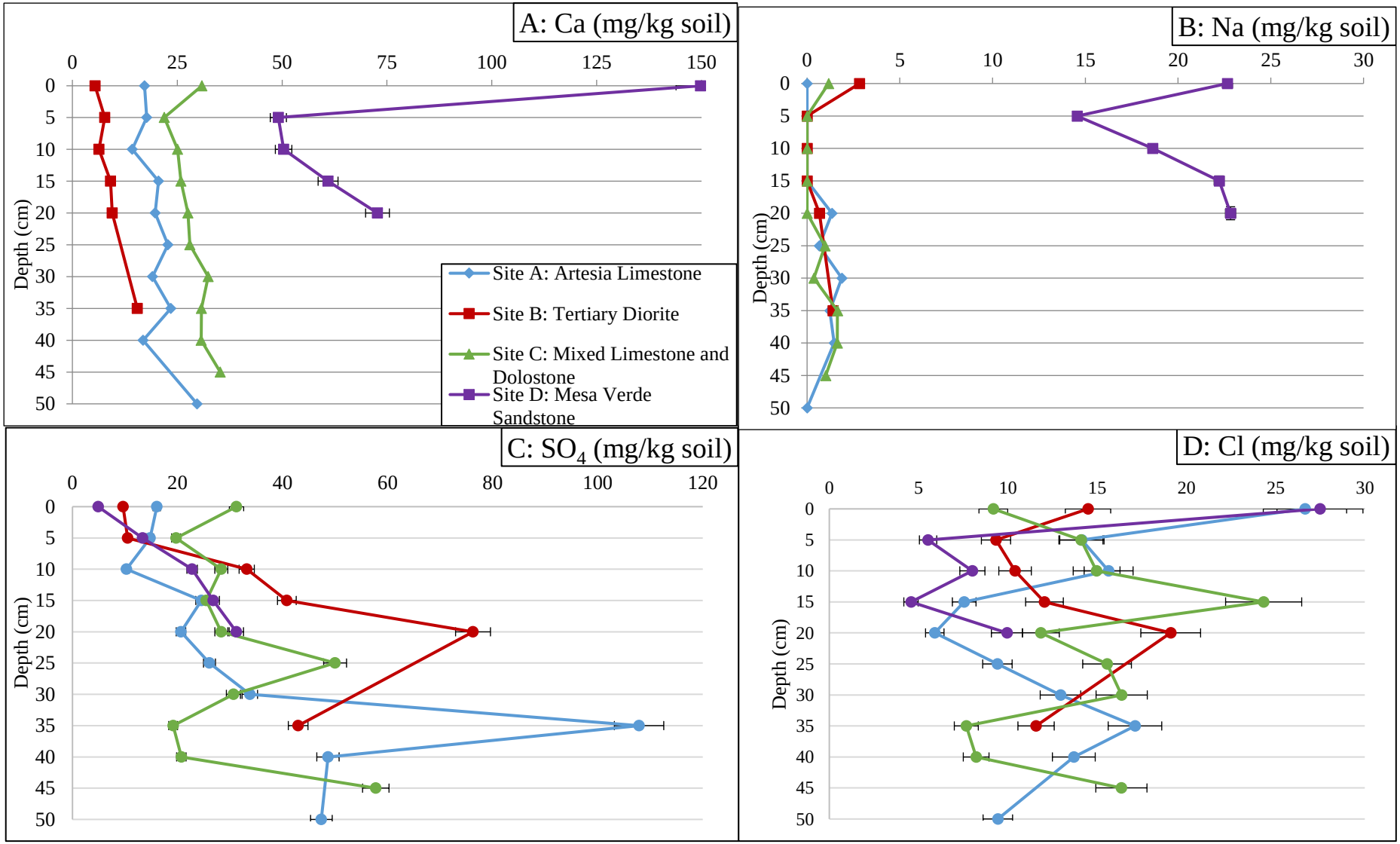

Figure 6: Variation of soluble ions in water leachate soil samples with depth: (A) Ca, (B) Na, (C) SO_4, and (D) Cl.

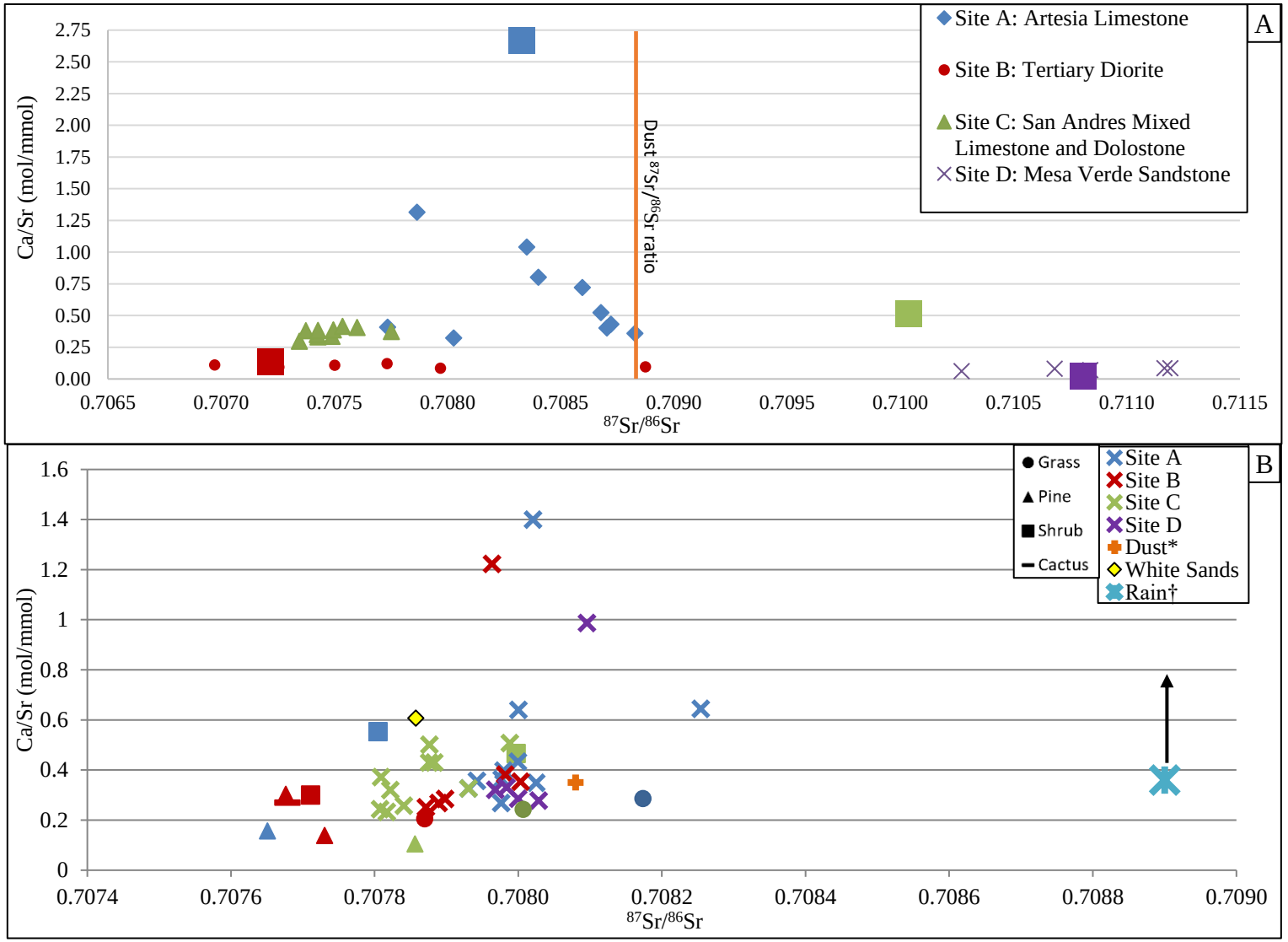

Figure 7: Variation of Ca/Sr as a function of $^{87}Sr/^{86}Sr$ in (A) bulk soil, rock, and dust samples and (B) all water leachate and plant samples. The deepest sample in each weathering profile (labelled as squares) in 6a indicate bedrock samples at each site. Shapes of plant samples in 5b and 5d indicate grass (circles,) pines (triangles,) shrubs (squares,) and cacti (dashes.)
*Dust leachate contains some rain water.
† Rain data from Capo and Chadwick (1999) suggests minimum Ca/Sr ratio and regional $^{87}Sr/^{86}Sr$ ratios.

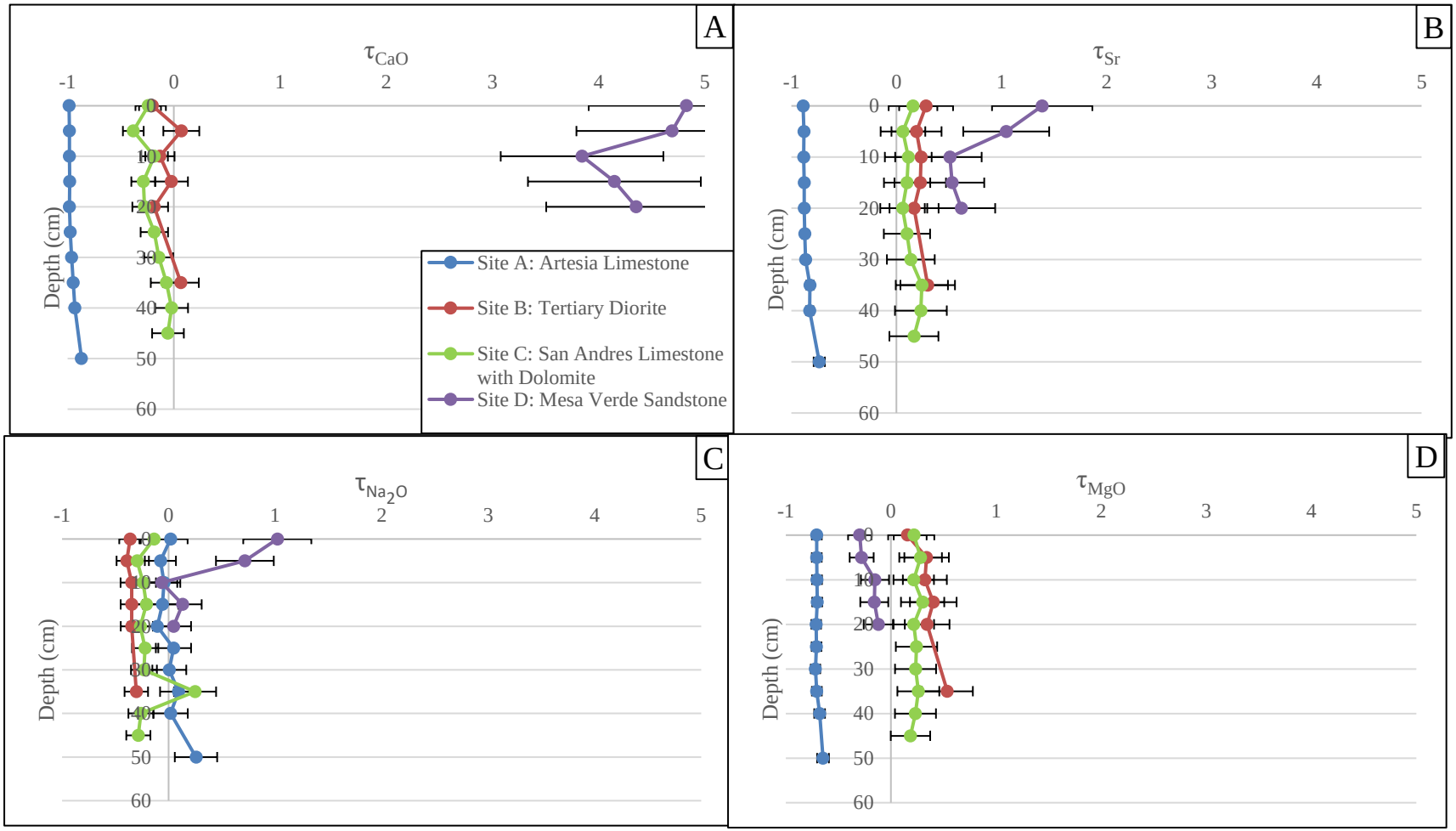

Figure 8: depth variation in mass balance transfer, coefficient τ of (A) calcium oxide, (B) strontium, (C) sodium oxide, and (D) magnesium oxide.

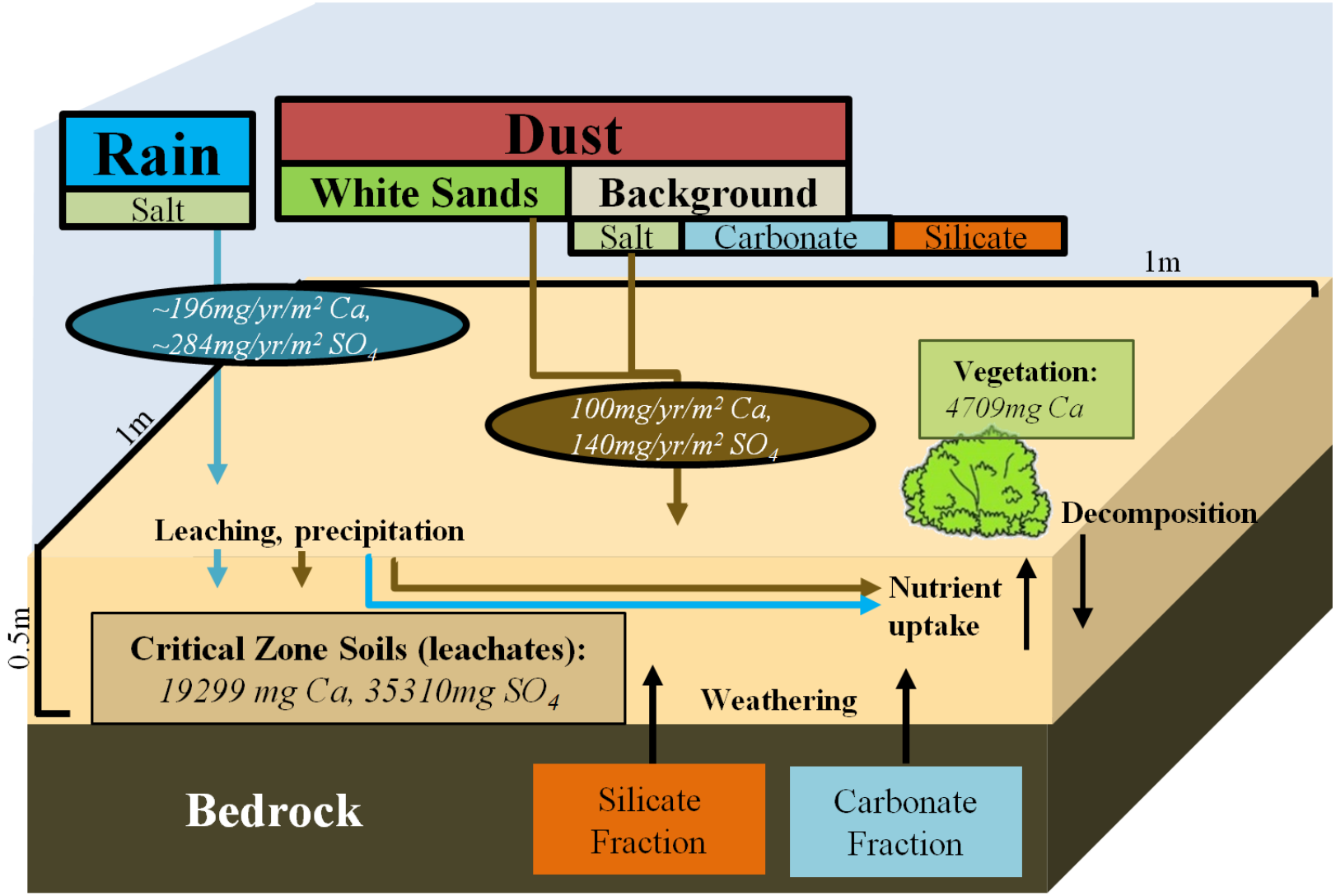

Figure 9: Schematic plot to show all known soluble calcium and sulfate fluxes in the critical zone at White Mountain, New Mexico. Rain volume derived from precipitation data from the National Trends Network (NTN) site in Mayhill, New Mexico.

8. WORKS CITED

Abouchami, W., Näthe, K., Kumar, A., Galer, S.J.G., Jochum, K.P., Williams, E., Horbe, A.M.C., Rosa, J.W.C., Balsam, W., Adams, D., Mezger, K., and Andreae, M.O., 2013, Geochemical and isotopic characterization of the Bodélé Depression dust source and implications for transatlantic dust transport to the Amazon Basin: Earth and Planetary Science Letters, v. 380, p. 112–123.

Aciego, S.M., Riebe, C.S., Hart, S.C., Blakowski, M.A., Carey, C.J., Aarons, S.M., Dove, N.C., Botthoff, J.K., Sims, K.W.W. and Aronson, E.L., 2017. Dust outpaces bedrock in nutrient supply to montane forest ecosystems. Nature Communications 8:14800.

Adler, P., Cumming, J., Arora, R., 2009, Nature of mineral nutrient uptake by plants: Agricultural Science, v. 1.

Allmendinger, R. and Titus, F., 1973, Regional hydrology and evaporative discharge as a present-day Source of Gypsum at White Sands National Monument, New Mexico, New Mexico Bureau of Mines and Mineral Resources, Open file report 55.

Arendt, C.A., Aciego, S.M., and Hetland, E.A., 2015, An open source Bayesian Monte Carlo isotope mixing model with applications in Earth surface processes: BMC ISOTOPE MIXING MODEL: EARTH SURFACE: Geochemistry, Geophysics, Geosystems, v. 16, no. 5, p. 1274–1292, doi: 10.1002/2014GC005683.

Baddock, M.C., Gill, T.E., Bullard, J.E., Acosta, M.D., and Rivera Rivera, N.I., 2011, Geomorphology of the Chihuahuan Desert based on potential dust emissions: Journal of Maps, v. 7, no. 1, p. 249–259.

Baddock, M.C., Ginoux, P., Bullard, J.E., and Gill, T.E., 2016, Do MODIS-defined dust sources have a geomorphological signature?: Geomorphology and Dust Emission: Geophysical Research Letters, v. 43, no. 6, p. 2606–2613.

Boy, J., and Wilcke, W., 2008, Tropical Andean forest derives calcium and magnesium from Saharan dust: Base Metal Deposition in Tropical Forest: Global Biogeochemical Cycles, v. 22, no. 1.

Bozlaker, A., Prospero, J. M., Fraser, M. P., and Chellam, S. , 2013. Quantifying the contribution of long-range Saharan dust transport on particulate matter concentrations in Houston, Texas, using detailed elemental analysis. Environmental Science and Technology 47(18): 10179-10187.

Brantley, S.L., Goldhaber, M.B., and Ragnarsdottir, K.V., 2007, Crossing disciplines and scales to understand the critical zone: Elements, v. 3, no. 5, p. 307–314.

Baddock, M.C., Gill, T.E., Bullard, J.E., Acosta, M.D., and Rivera Rivera, N.I., 2011, Geomorphology of the Chihuahuan Desert based on potential dust emissions: Journal of Maps, v. 7, no. 1, p. 249–259.

Bristow, C.S., Hudson-Edwards, K.A., and Chappell, A., 2010, Fertilizing the Amazon and equatorial Atlantic with West African dust: AFRICAN FERTILIZER FOR AMAZON AND ATLANTIC: Geophysical Research Letters, v. 37, no. 14.

Capo, R.C., and Chadwick, O.A., 1999, Sources of strontium and calcium in desert soil and calcrete: Earth and Planetary Science Letters, v. 170, no. 1, p. 61–72.

Climate data for cities worldwide - Climate-Data.org.

Czaja, A., Estrada-Rodríguez, J.L., and Flores Olvera, H., 2014, The Gypsum Dunes of Cuatrociénegas Valley, Mexico – A Secondary Sabkha Ecosystem with Gypsophytes, *in* Khan, M.A., Böer, B., Öztürk, M., Al Abdessalaam, T.Z., Clüsener-Godt, M., and Gul, B. eds., Sabkha Ecosystems: Volume IV: Cash Crop Halophyte and Biodiversity Conservation, Springer Netherlands, Dordrecht, p. 81–92.

Derry, L A and Chadwick, O A, 2007, Contributions from Earths Atmosphere to Soils. Elements , v. 3, p. 333-338.

Faure, G., 1998, Principles and Applications of Geochemistry: Prentice Hall, Upper Saddle River, N.J.

Francis, R, 1964, Chemistry of Chemistry of water of a section of the eastern flank of the Sacramento Mountains, Lincoln and Otero Counties, New Mexico*:* New Mexico Geological Society Fall Field Conference Guidebook, v. 15, p. 161-170.

Fryberger, S., 2001, Geological Overview of White Sands National Monument: accessible at http://nature.nps.gov/geology/parks/whsa/geows/index.htm

New Mexico Bureau of Geology and Mineral Resources, 2003, Geologic Map of New Mexico, Scale 1:500,000. accessible at https://geoinfo.nmt.edu/publications/maps/geologic/state/home.cfml

Gill, T.E., 1996, Eolian sediments generated by anthropogenic disturbance of playas: human impacts on the geomorphic system and geomorphic impacts on the human system: Geomorphology, v. 17, no. 1–3, p. 207–228, doi: 10.1016/0169-555X(95)00104-D.

Graustein, W.C., and Armstrong, R.L., 1983, The Use of Strontium-87/Strontium-86 Ratios to Measure Atmospheric Transport into Forested Watersheds: Science, v. 219, no. 4582, p. 289–292.

Grousset, F.E., Biscaye, P.E., 2005, Tracing dust sources and transport patterns using Sr Nd and Pb isotopes. Chem Geol 222:149–167

Haga, H., Moriishida, T., Morishita, N., Fujimoto, T., 2017, Properties of small instream wood as a logjam clogging agent: Implications for clogging dynamics based on wood density, water content, and depositional environment: Geomorphology, v. 296.

Hahnenberger M, Nicoll K, 2012, Meteorological characteristics of dust storm events in the eastern Great Basin of Utah, U.S.A. Atmos Environ 60:601–612

Hanks, J.P., and Dick-Peddie, W.A., 1974, Vegetation Patterns of the White Mountains, New Mexico: The Southwestern Naturalist, v. 18, no. 4, p. 371.

Harouaka, K., Eisenhauer, A., and Fantle, M.S., 2014, Experimental investigation of Ca isotopic fractionation during abiotic gypsum precipitation: Geochimica et Cosmochimica Acta, v. 129, p. 157–176.

Hoidale, G.B., and Smith, S.M., 1968, Analysis of the giant particle component of the atmosphere over an interior desert basin: Tellus, v. 20, no. 2, p. 251–268.

Horton, J.D., C.A. San Juan, and D.B. Stoeser. The State Geologic Map Compilation (SGMC) geodatabase of the conterminous United States. doi: 10.3133/ds1052. U.S. Geological Survey Data Series 1052. [133]

Huneeus, N., Schulz, M., Balkanski, Y., Griesfeller, J., Prospero, J., Kinne, S., Bauer, S., Boucher, O., Chin, M., Dentener, F., Diehl, T., Easter, R., Fillmore, D., Ghan, S., et al., 2011, Global dust model intercomparison in AeroCom phase I: Atmospheric Chemistry and Physics, v. 11, no. 15, p. 7781–7816.

Jin, L., Ravella, R., Ketchum, B., Bierman, P. R., Heaney, P., White, T., and Brantley, S.L. (2010) Mineral weathering and elemental transport during hillslope evolution at the Susquehanna/Shale Hills Critical Zone Observatory. Geochimica et Cosmochimica Acta 74, 3669-3691.

KellerLynn, K. 2012. White Sands National Monument: geologic resources inventory report. Natural Resource Report NPS/NRSS/GRD/NRR—2012/585. National Park Service, Fort Collins, Colorado, USA.

Kelley, C. and Thompson, T.B., 1964, Tectonics and general geology of the Ruidoso--Carrizozo region, central New Mexico, New Mexico Geological Society Fall Field Conference Guidebook, v. 15, p. 110-121.

Kocurek, G., M. Carr, R. Ewing, K. G. Havholm, Y. C. Nagar, and A. K. Singhvi, 2007, White Sands Dune Field, New Mexico: Age, dune dynamics and recent accumulations. Sedimentary Geology 197:313-331

Konter, J. G., Storm, L.P., 2014. High precision $^{87}Sr/^{86}Sr$ measurements by MC-ICP-MS, simultaneously solving for Kr interferences and mass-based fractionation. Chemical Geology, 385, 26-34. doi:10.1016/j.chemgeo.2014.07.009

Knippertz, P., and Stuut, J.-B.W. (Eds.), 2014, Mineral Dust: Springer Netherlands, Dordrecht.

Kumar, A., Abouchami, W., Galer, S.J.G., Garrison, V.H., Williams, E., and Andreae, M.O., 2014, A radiogenic isotope tracer study of transatlantic dust transport from Africa to the Caribbean: Atmospheric Environment, v. 82, p. 130–143, doi: 10.1016/j.atmosenv.2013.10.021.

Langford, R.P., 2003, The Holocene history of the White Sands dune field and influences on eolian deflation and playa lakes, Quarternary International 104, 31-39.

Langford, R.P., Gill, T.E., and Jones, S.B., 2016, Transport and mixing of eolian sand from local sources resulting in variations in grain size in a gypsum dune field, White Sands, New Mexico, USA: Sedimentary Geology, v. 333, p. 184–197, doi: 10.1016/j.sedgeo.2015.12.010.

Lanphere, M., 2001, Radiometric Dating A2 - Meyers, Robert A., *in* Encyclopedia of Physical Science and Technology (Third Edition), Academic Press, New York, p. 721–730.

Lawrence, C.R., Reynolds, R.L., Ketterer, M.E., and Neff, J.C., 2013, Aeolian controls of soil geochemistry and weathering fluxes in high-elevation ecosystems of the Rocky Mountains, Colorado: Geochimica et Cosmochimica Acta, v. 107, p. 27–46, doi: 10.1016/j.gca.2012.12.023.

Likens, G., Driscoll, C., Buso, D., Mitchell, M., Lovett, G., Bailey, S., Siccama, T.G., Reiners, W.A., and Alewell, C., 2002, The biogeochemistry of sulfur at Hubbard Brook: Biogeochemistry, v. 60, p. 235–316.

Marchand, D.E., 1970, Soil contamination in the White Mountains, eastern California: Geological Society of America Bulletin, v. 81, no. 8, p. 2497–2506.

Martin, W., 1964, Some aspects of the natural history of the Capitan and Jicarilla mountains and Sierra Blanca region of New Mexico, New Mexico Geological Society Fall Field Conference Guidebook, v. 15, p. 171-176.

Muhs D., Budahn J., Johnson D., Reheis ., Beann J., Skipp G., Fisher E, Jones JA, 2008, Geochemical evidence for airborne dust additions to soils in Channel Islands National Park California. Geol Soc Am Bull 120:106–126

Muhs D., Budahn J., Prospero J., Skipp G., Herwitz S., 2012, Soil genesis on the island of Bermuda in the Quaternary: the importance of African dust transport and deposition. J Geophys Res 117, F03025

Nasa Earth Observatory, Dust Plume from White Sands : Natural Hazards, 2012, accessible at http://earthobservatory.nasa.gov/NaturalHazards/view.php?id=77294

National Trends Network, NADP: Precipitation data accessible at http://nadp.sws.uiuc.edu/data/sites/siteDetails.aspx?net=NTN&id=NM08

Neher, D.A., Lewins, S.A., Weicht, T.R., Darby, B. J., 2009, Microarthropod communities associated with biological soil crusts in the Colorado Plateau and Chihuahuan deserts: Journal of Arid Environments, v. 73, Issues 6–7, Pages 672-677.

Pelt, E., Chabaux, F., Stille, P., Innocent, C., Ghaleb, B., Gérard, M., and Guntzer, F., 2013, Atmospheric dust contribution to the budget of U-series nuclides in soils from the Mount Cameroon volcano: Chemical Geology, v. 341, p. 147–157, doi: 10.1016/j.chemgeo.2013.01.008.

Perez, A.E. 2008, Application of integrated remote sensing and GIS technologies to geoenvironmental issues in far west Texas and southern New Mexico, Ph.D. dissertation, University of Texas at El Paso

Perez, A.E., and Gill, T.E., 2009, Salt Flat Basin's contribution to regional dust production and potential influence on dry deposition in the Guadalupe Mountains (Texas, USA): Natural Resources and Environmental Issues, v. 15, p. 117.

Pett-Ridge, J.C., Derry, L.A., and Barrows, J.K., 2009, Ca/Sr and 87Sr/86Sr ratios as tracers of Ca and Sr cycling in the Rio Icacos watershed, Luquillo Mountains, Puerto Rico: Chemical Geology, v. 267, no. 1-2, p. 32–45, doi: 10.1016/j.chemgeo.2008.11.022.

Prospero, J.M., 2002, Environmental characterization of global sources of atmospheric soil dust identified with the NIMBUS 7 Total Ozone Mapping Spectrometer (TOMS) absorbing aerosol product: Reviews of Geophysics, v. 40, no. 1, doi: 10.1029/2000RG000095.

Reynolds, R., Belnap, J., Reheis, M., Lamothe, P., and Luiszer, F., 2001, Aeolian dust in Colorado Plateau soils: Nutrient inputs and recent change in source: Proceedings of the National Academy of Sciences, v. 98, no. 13, p. 7123–7127, doi: 10.1073/pnas.121094298.

Reynolds, R., Neff, J., Reheis, M., and Lamothe, P., 2006, Atmospheric dust in modern soil on aeolian sandstone, Colorado Plateau (USA): Variation with landscape position and contribution to potential plant nutrients: Geoderma, v. 130, no. 1–2, p. 108–123.

Reheis, M. and Kihl, R., 1995, Dust Deposition in southern Nevada and California (1984-1989); relations to climate, source area, and source lithology. Journal of Geophysical Research, 100 (D5), p. 8893-918.

Rivas, J.A., Gill, T.E., Walsh, E.J., and Wallace, R.L., 2014. Characterization of dust transported to El Paso, Texas. Abstracts of the 18th Jount Conference on the

Applications of Air Pollution Meteorology with the AWMA, American Meteorological Society Annual Meeting, Atlanta, GA, February 2014, no. 236614.

Rivera Rivera, N.I., Gill, T.E., Bleiweiss, M.P., and Hand, J.L., 2010, Source characteristics of hazardous Chihuahuan Desert dust outbreaks: Atmospheric Environment, v. 44, no. 20, p. 2457–2468.

Sohn, R.A., 2005, A general inversion for end-member ratios in binary mixing systems: General Inversion for Binary Mixing: Geochemistry, Geophysics, Geosystems, v. 6, no. 11.

Swap, R., et al., 1992. Saharan dust in the Amazon Basin. Tellus 44B, 133-149.

Stewart, B.W., Capo, R.C., and Chadwick, O.A., 1998, Quantitative strontium isotope models for weathering, pedogenesis and biogeochemical cycling: Geoderma, v. 82, no. 1–3, p. 173–195.

Szynkiewicz, A., Ewing, R.C., Moore, C.H., Glamoclija, M., Bustos, D., and Pratt, L.M., 2010, Origin of terrestrial gypsum dunes—Implications for Martian gypsum-rich dunes of Olympia Undae: Geomorphology, v. 121, no. 1–2, p. 69–83.

Tchakerian, V., and Pease, P., 2015, The Critical Zone in Desert Environments, *in* Developments in Earth Surface Processes, Elsevier, p. 449–472.

Trapp J.M., Millero, F.J., and Prospero, J.M., 2010. Temporal variability of the elemental composition of African dust measured in trade wind aerosols at Barbados and Miami. Marine Chemistry v. 120: p. 71- 82.

Veizer, J., 1989, Strontium Isotopes in Seawater through Time: Annual Review of Earth and Planetary Sciences, v. 17, no. 1, p. 141–167.

Vander Lee, B., Smith, R., and Bate, J, 2004, Ecological and Biological Diversity of the Lincoln National Forest in: Ecological and Biological Diversity of National Forests in Region 3. The Nature Conservancy.

Waterfall, U.T., 1946, Observations on the Desert Gypsum Flora of Southwestern Texas and Adjacent New Mexico: American Midland Naturalist, v. 36, no. 2, p. 456.

White, W.H., Hyslop, N.P., Trzepla, K., Yatkin, S., Rarig, R.S., Gill, T.E., and Jin, L., 2015, Regional transport of a chemically distinctive dust: Gypsum from White Sands, New Mexico (USA): Aeolian Research, v. 16, p. 1–10.

9. APPENDICES

Appendix A:

Lithium Metaborate Fusion Technique

- Add *0.100 or of -100 mesh samples* to a pre-weighed vials containing *1.00 gram. of lithium metaborate*.
- Shake vials by hand, gently but thoroughly mixing the two components.
- Dump contents of vials into a graphite crucibles and insert crucibles into an oven pre-heated to 900C.
- Pipette *100 mL of a 5% nitric acid* solution into watch glass covered Teflon beakers and add a stirring bar to each.
- After ten minutes at 1000°C (allow a few minutes for oven to return to 900°C), place beakers on magnetic stirrers and start then swirl the contents of the crucibles to pick up any uncoalesced beads and dump into beakers.
- After a few minutes, carefully examine the graphite crucibles for any remaining melt, scrape off if present and add to beakers.
- Stir at least 15 minutes and transfer to polyethylene bottles for storage.
- BEFORE RUNNING samples, dilute with 5% HNO_3 by 1:10.

Tips and hints

- If melt sticks to graphite crucible and cannot be completely scraped out and dissolved, a smaller sample size will have to be used.
- Difficult samples such as zircons and high iron ores, will sometimes dissolved when fused in a 1:3 mix of sample to SiO_2 or Al_2O_3. (e.g. .050 gram sample + 0.150 gram SiO_2 +1.000 gram $LiBO_2$.)
- This technique will not work for elements that are volatile at 900C.
- Standards may be made by preparing a lithium metaborate matrix solution and using this to dilute down stock solutions.
- Standards may also be prepared by fusing known rock and/or ore standards (e.g. U.S.G.S. rock standards), along with the samples.
- Do not mix samples and standards prepared more than four weeks apart.
- Crucibles should be thoroughly wiped out with kimwipes in between samples.
- **Wear proper protection**.

APPENDICES REFERENCES:

Suhr, N.H. and Ingamells, C.O. (1966), Solution Technique for Analysis of Silicates, Anal. Chem., 38, 730-734.

Medlin, J.H., Suhr, N.H., and Bodkin, J.B. (1969), Atomic Absorption Analysis of Silicates Employing $LiBO_2$ Fusion, Atomic Absorption Newsletter, Vol. 8, No. 2, 25-29.

Ingamells, C.O. (1970), Lithium Metaborate Flux in Silicate Analysis, Anal. Chim. Acta, 52, 323-334.

Feldman, C. (1983), Behavior of Trace Refractory Minerals in the Lithium Metaborate Fusion-Acid Dissolution Procedure, Anal. Chem., Vol 55, No. 14, 2451-2453

Appendix B:

Total sample digestion procedure for Sr isotope analysis.

1. Weigh 100 mg of sample into a clean 30ml Teflon beaker. (If the sample is not enough, scale down to 50mg of sample).
2. Add 1ml of concentrated HNO_3 (distilled or pure acid)
3. Using a new pipette tip, add 2ml of pure concentrated HF (Be extremely careful this is a dangerous acid). Working in the fume hood while adding this acid is recommended
4. Close the beakers tightly and put them on ultrasonic machine for 30min
5. Place the tightly capped beakers on a hot plate at 90^0 C in the cleanroom overnight. Check if all the solid material is dissolved.
6. If the sample is completely digested, evaporate the samples at 100^0C to dryness (check the drying samples frequently, often completely dry samples are blown away).
7. To the dry samples, add 1ml saturated boric acid, 2ml of 6N HCl, and 3ml deionized water (you should see a yellow solution "cocktail"). Cap the beakers tightly and place them on the hot plate at 100^0C for 24-48 hrs.
8. Once the samples are digested (no solid material at bottom of the beaker), evaporate the samples to dryness. Again, check the drying samples frequently.
9. Dissolve the dry samples in 0.5-1ml of 3.5N HNO_3 and evaporate to dryness.
10. Re-dissolve the sample in 0.5 ml of 3.5N HNO_3; this solution is ready for column chemistry.

Appendix C:

Dust Loss on Ignition (LOI)

Sample	Site	Date Range	Initial weight (mg)	Post-LOI weight (mg)	% OM
DA	A	4/9/2016-9/24/2016	178.8	108.2	39.5
DB	A	2/1/2016-9/24/2016	103.2	41.6	59.7
DC	C	4/9/2016-9/24/2016	579.5	342.9	40.8
DD	C	4/9/2016-9/24/2017	185.5	113	39.1
DE	A	2/1/2016-4/9/2016	49.3	28.2	42.8
DF	C	4/9/2016-9/24/2016	238.2	176.6	25.9
DG	A	1/20/2017-6/3/2017	365.81	239.9	34.4
DH	A	1/20/2017-6/3/2017	45	27.8	38.2
DI	C	1/20/2017-6/3/2017	485.71	397.8	18.1
DJ	C	1/20/2017-6/3/2017	344.7	255.1	26.0

Appendix D:

Duplicates and Checks for Quality Control of Soil Samples

Sample ID	Duplicate Type	Al_2O_3 %	CaO %	Fe_2O_3 %	K_2O %	MgO %	MnO %	Na_2O %	TiO_2 %	Ba (ppm)	Sr (ppm)	Zr (ppm)
A00 - D	Procedure	12.8	5.38	4.13	3.39	1.27	0.08	2.19	0.76	648.13	266.71	288.6
A10 – D	Analytical	12.28	6.95	4.04	3.21	1.19	0.07	1.96	0.74	1030.71	276.8	328.62
A15 - D	Analytical	13.01	7.97	4.28	3.28	1.24	0.08	1.96	0.77	989.39	294.82	334.87
A30 – D	Analytical	11.95	13.22	3.63	3.12	1.03	0.06	1.83	0.68	1202.73	293.1	404.19
A35 – D	Procedure	13.71	21.39	4.17	3.71	1.16	0.07	2.2	0.74	720.69	367.52	448.57
A40 – D	Analytical	10.26	20.37	3.42	2.68	1.01	0.05	1.61	0.58	768.1	315.71	305.1
B05 – D	Analytical	15.02	2.49	4.97	3.76	1.2	0.11	2.66	0.93	587.39	314.77	420.97
B10 – D	Procedure	15.11	1.95	5.03	3.74	1.16	0.1	2.72	0.89	886.28	306.45	371.85
B20 – D	Procedure	15.42	1.85	5.06	3.81	1.08	0.09	2.72	0.9	881.52	307.04	315.34
B35 – D	Analytical	16.91	2.5	5.35	4.18	1.25	0.1	3.02	0.92	984.07	331.1	453.38
Blank	N/A	1.35	0.97	0.27	0.09	0.16	0	0.01	0.02	38.75	18.29	0

10. VITA

Patrick Richard Rea was born and raised in central Pennsylvania. He obtained a B.S. in Geology from Juniata College in Huntingdon, PA. While studying at Juniata, he was a research assistant, as well as a teaching assistant and tutor for multiple geology, chemistry, and environmental science classes. He also interned as an environmental technician at Mountain Research, LLC, and studied abroad at the University of Newcastle, NSW, Australia over the course of his undergraduate degree. In graduate school, Patrick presented in two UTEP geological sciences colloquium and at the 2017 national GSA annual meeting. He also was a member of the 2016 world champion AAPG Imperial Barrel Award team, and was involved in the student AAPG branch as secretary from 2016-2017. From June of 2016 to December of 2016, he interned at NASA Langley Research Center's Atmospheric Science Data Center as a junior data scientist, supporting the data distribution team and performing data assessment of remote sensing data.

Permanent email address: Patrick.r.rea@gmail.com

This thesis was typed by Patrick R. Rea.